Reduced-Dimension Blind Space-Time 2-D Rake Receivers for DS-CDMA Communication Systems

Yung-Fang Chen, Michael D. Zoltowski, *Fellow, IEEE*, Javier Ramos, Chanchal Chatterjee, and Vwani P. Roychowdhury

***Abstract*—Blind space-time RAKE receivers for classical DS-CDMA that cancel strong multiuser access interference while optimally combining the desired user's multipath are presented. The delay spread is assumed to be fraction of a symbol interval as in the IS-95 CDMA standard. The post-correlation symbol interval is segmented into that which encompasses the RAKE fingers and that away from the RAKE fingers. The signal-plus-interference and interference-alone space-time correlation matrices are estimated during the former and latter, respectively. Reduced-dimension space-time RAKE receivers are investigated for alleviation of the computational burden of computing the largest generalized eigenvector of the resulting matrix pencil. Theoretical analysis and supporting simulations reveal that if the space and time compressing transformations are designed judiciously, reduced-dimension two-dimensional (2-D) RAKE receivers offer faster convergence at the expense of only a slight loss in asymptotic signal-to-interference-plus-noise ratio (SINR) relative to the full-dimension space-time RAKE receiver. Applications to the IS-95 uplink are also presented along with supporting simulations.**

***Index Terms*—Array signal processing, digital communication, pseudonoise coded communications.**

I. Introduction

THE GOAL of a space-time or two-dimensional (2-D) RAKE receiver [3] is to optimally combine the multipath for the desired user across both space and time while simultaneously canceling co-channel interference: both strong multiuser access interference (MUAI) and narrowband interferers. The development begins with a brief overview of blind 2–D RAKE receivers.

Manuscript received September 14, 1998; revised August 11, 1999. This work was supported by the Air Force Office of Scientific Research under Contract F49620-97-1-0275, the National Science Foundation under Grant MIPS-9708309, and the Army Research Office Focused Research Initiative under Grant DAAH04-95-1-0246. The associate editor coordinating the review of this paper and approving it for publication was Dr. Lal C. Godara.

Y.-F. Chen is with Lucent Technologies, Whippany, NJ 07981 USA (e-mail: ychen3@lucent.com).

M. D. Zoltowski is with the School of Electrical and Computer Engineering, Purdue University, West Lafayette, IN 47907-1285 USA (e-mail: mikedz@ecn.purdue.edu).

J. Ramos is with Carlos III University of Madrid, Madrid, Spain (e-mail: javier@tsc.uc3m.es).

C. Chatterjee is with GDE Systems, San Diego, CA 92127 USA (e-mail: Chanchal.Chatterjee@marconi-is.com).

V. P. Roychowdhury is with the Electrical Engineering Department, University of California, Los Angeles, Angeles, CA 90095-1594 USA (e-mail: vwani@ee.ucla.edu).

Publisher Item Identifier S 1053-587X(00)03333-X.

A. Space-Only Processing

The reduced-dimension 2-D RAKE receivers proposed in Section III have their roots in the pioneering work of Suard *et al.*on the use of *precorrelation* and *post-correlation* spatial correlation matrices reported in their seminal papers [2], [7]. Refer to Fig. 2. For a given antenna, the output of the matched filter is the cross-correlation between the signal received at the antenna and the spreading waveform of the desired user. The basic idea behind the blind adaptive beamforming scheme proposed in [2] and [7] is as follows. If the processing gain is large, the contribution of the desired user to the composite signal (including MUAI and receiver noise) at the input to the correlator is small relative to the contribution of the desired user to the output of the correlator during the time interval where the RAKE fingers occur.

Suard *et al.* proposed forming spatial correlation matrices *pre-* and *post-correlation*, i.e., before and after passing the received signal through an FIR filter composed of samples of the spreading waveform for the desired user. Asymptotically, the contribution to either spatial correlation matrix due to interference is the same. However, the *post-correlation* matrix has an additive contribution from the desired signal that is much larger than the corresponding contribution to the *pre-correlation* spatial correlation matrix by a factor equal to the processing gain. In the case of a negligible multipath time-delay spread, this additive contribution is rank one. Suard *et al.* proposed approximating the direction-of-arrival (DOA) vector for the desired user as the "largest" eigenvector of the difference between the *pre-* and *post-correlation* spatial matrices. Pre-multiplying this estimate of the desired user's DOA vector by the inverse of the pre-correlation spatial correlation matrix yielded the beamforming weight vector to be applied across the array aperture in their scheme.

B. Direct Space-Time Extension of Spatial Scheme of Suard et al.

The Suard *et al.* novel *pre-* and *post-correlation* processing scheme was the first adaptive algorithm that exploited the large processing gain achieved by knowing the desired user's code to blindly estimate a beamforming weight vector that canceled MUAI. Liu and Zoltowski [4] proposed a space-time extension of the Suard *et al.*pioneering scheme: Form space-time correlation matrices before and after matched filtering with samples of the spreading waveform of the desired user. The space-time vector associated with the desired user is estimated as the "largest" eigenvector of the difference between the *pre-* and *post-correlation* space-time correlation matrices.

The space-time weights applied to the time samples encompassing the RAKE fingers is computed by premultiplying this estimate of the desired user's space-time vector by the inverse of the *pre-correlation* space-time correlation matrix. However, whereas the spatial characteristics of the interferers are not changed by passing the received signal at each antenna through a matched filter composed of samples of the spreading waveform of the desired user, the temporal characteristics are generally altered. Thus, the respective asymptotic forms of the *pre-* and *post-correlation* space-time correlation matrices due to interference alone are generally different, thereby violating the basic premise of this extension of Suard's scheme.

C. Post-Correlation Symbol Interval Segmentation

In [5], Wong and Zoltowski *et al.* proposed forming the 2-D RAKE receiver weights as follows. Referring to Fig. 2, after passing the output of each antenna through a matched filter, whose impulse response is an oversampled version of the time-reverse of the spreading waveform of the desired user, one estimates the signal plus interference (plus noise) space-time correlation matrix $\mathbf{K}_{S+I+N}$ during that portion of the bit interval where the RAKE fingers occur and the interference (plus noise) alone space-time correlation matrix $\mathbf{K}_{I+N}$ during that portion of the bit interval away from the fingers. The criterion for finding space-time weights that maximize signal-to-interference-plus-noise ratio (SINR) is

$$\underset{\mathbf{w}}{\text{Maximize}}\ \frac{\mathbf{w}^H\mathbf{K}_{S+I+N}\mathbf{w}}{\mathbf{w}^H\mathbf{K}_{I+N}\mathbf{w}} = \underset{\mathbf{w}}{\text{Maximize}}\ \frac{\mathbf{w}^H\mathbf{K}_{S}\mathbf{w}}{\mathbf{w}^H\mathbf{K}_{I+N}\mathbf{w}} + 1. \tag{1}$$

Let M be the number of antennas and N_s the number of time samples per antenna extracted near the "RAKE fingers." It was shown that the $MN_s \times 1$ weight vector $\mathbf{w}_{\text{opt}}$ yielding the optimum SINR for bit decisions is the "largest" generalized eigenvector of the matrix pencil $\{\mathbf{K}_{S+I+N}, \mathbf{K}_{I+N}\}$.

The basic idea is that the processing gain is large enough so that the interference dominates over that portion of the bit interval away from the RAKE fingers (by a couple of chips or so). Approximate bit synchronization is an important assumption underlying this scheme. It is assumed that one knows roughly where the fingers are located in time. It is also assumed that they encompass a fraction of the bit interval, implying the multipath delay spread is small compared with the bit duration. Approximate bit synchronization may be achieved by first employing [6] or applying the pre- and post-correlation spatial-only processing schemes [2], [7] to effect a beam that is roughly pointed toward the desire user with nulls toward the dominant interferers, followed by a simple energy detector. Note that both $\mathbf{K}_{S+I+N}$ and $\mathbf{K}_{I+N}$ are formed post-correlation so that there is no issue of altering the temporal characteristics of the interferers. However, the scheme requires multiplying by the code and summing over a large number of delays that are much greater than the delay spread.

Complexity Issues: Taking a cue from either the IS-95 standard or the coarse acquisition code embedded in the GPS signal, suppose that the chip duration is approximately 1 μs. Experimental measurements in an urban cellular environment reveal that the worst case time delay spread $\tau_{\max}$ due to multipath is on the order of 10 μs [8]. Sampling two times per chip over 10 μs yields space-time correlation matrices of dimension $20M \times 20M$ it is 160×160 in the case of $M = 8$ antennas. If the multipath time-delay spread is 20 μs, as in the case with Denver, CO, and other cities located near mountainous regions, the space-time correlation matrices would be of dimension 320×320 with $M = 8$ antennas and sampling two times per chips.

The large dimensionality of the space-time correlation matrix pencil implies high computational complexity and slow convergence rate, which negatively affects operation under mobile channel conditions. These are the primary motivating factors for the development of reduced dimension space-time 2-D RAKE receivers offering the following advantages [12]: 1) reduced computational complexity and 2) faster convergence to near optimum SINR in the symbol decision statistic.

D. Application to the IS-95 Uplink

The CDMA system proposed in the IS-95 cellular standard uses time-varying spreading waveforms and 64-ary orthogonal signalling on the uplink: a significant departure from the BPSK modulation and time-invariant spreading assumed in [9] and [10]. A base-station antenna array receiver with M-ary orthogonal modulation was proposed in [13], which is commensurate with the IS-95-based CDMA system. However, this receiver requires estimation of the path delays for the desired user. These parameters may be difficult to estimate without strict power control due to the "near-far" problem. In addition, their estimation and tracking requires a substantial computational overhead. In addition, note that the MMSE interference suppression scheme in [1] was only applicable to short spreading codes, which does not apply to the IS-95 uplink structure where the signal subspace spanned by the code of desired user varies from symbol to symbol. Our processing schemes can be applied to either long or short signature sequence DS-CDMA communication systems; the application of our blind 2-D RAKE receiver to the IS-95 uplink is developed and supported through simulations.

II. Space-Time Data Model

The $M \times 1$ array snapshot vector $\mathbf{x}(t)$ containing the outputs of each of the M antennas comprising the array at time t is modeled as

$$\mathbf{x}(t) = \sum_{k=1}^{P} \rho_k \sum_{m=0}^{N_b-1} \mathbf{a}\left(\theta_k^d\right) D(m)c(t - mT_b - \tau_k) + \sum_{i=1}^{J} \sum_{m=0}^{N_b-1} \mathbf{a}(\theta_i)\sigma_i D_i(m)c_i(t - mT_b) + \mathbf{n}_w(t) \tag{2}$$

where $\mathbf{a}(\theta)$ is the spatial response of the array. For the sake of notational simplicity, we here assume that the spatial response vector depends on a single directional parameter θ, which is the DOA of a given source. However, no model is assumed for $\mathbf{a}(\theta)$ in the algorithm to be presented; the algorithm works for any array geometry, where

- $1/T_b$ symbol rate common to all sources;
- P number of different paths from which the signal of interest (SOI) arrives;

θ_k^d directions associated with the kth path;
τ_k corresponding relative delay of the kth path;
ρ_k complex amplitude of the kth multipath arrival for the SOI at the reference element.

$D(m)$ and $D_i(m)$ are the digital information sequences for the SOI and MUAI sources, respectively. J broadband interferers (MUAI) impinge on the array. σ_i is the complex amplitude of the ith interferer at the reference element of the array. $c(t)$ and $c_i(t)$ are the spreading waveforms for the SOI and ith MUAI, respectively. The vector $\mathbf{n}_w(t)$ contains white noise. N_b is the number of bits over which all parameters characterizing the model in (2) are assumed to be constant. N_b might be quite small in cases of rapidly evolving dynamics. The spreading waveform for the ith MUAI is modeled as

$$c_i(t) = \sum_{l=0}^{N_c-1} s_i(l) p_c\left(t - lT_c - T_{\text{off}_i}\right) \tag{3}$$

where

$(1/T_c)$ chip rate;
$s_i(l)$ PN sequence;
$p_c(t)$ chip waveform assumed common to all sources;
N_c number of chips per bit common to all MUAI's (without loss of generality);
T_{off_i} timing offset of the ith MUAI[1] relative to the desired user.

The spreading waveform for the desired source $c(t)$ is defined similarly but with a different PN sequence.

The received signal at each antenna is sampled at a rate L_c/T_c, where L_c is the number of samples per chip. The sampled output of each antenna is passed through a filter with impulse response $h[n] = c^*[-n]$, where $c[n] = c(nT_c/L_c)$. Denote the $N \times 1$ ($N = MN_s$) post-correlation space-time snapshot $\mathbf{x}_{\text{st}}[n] = [x_1[n], x_2[n], \ldots x_M[n], x_1[n+1], \ldots x_M[n+1], \ldots x_1[n+(N_s-1)], \ldots x_M[n+(N_s-1)]]^T$, where $N_s = \lceil (L_c\tau_{\max}/T_c) \rceil$ is the number of samples encompassing the multipath time delay spread, and $x_j[n]$ denotes the sample of the output of the jth antenna after the matched filter. The $N \times N$ signal plus interference (plus noise) space-time correlation matrix is estimated as

$$\hat{\mathbf{K}}_{S+I+N} = \frac{1}{N_b} \sum_{l=0}^{N_b-1} \mathbf{x}_{\text{st}}[lN_t]\mathbf{x}_{\text{st}}^H[lN_t] \tag{4}$$

where $N_t = N_c L_c$ is the total number of samples in one bit period. The interference (plus noise) space-time correlation matrix is estimated as

$$\hat{\mathbf{K}}_{I+N} = \frac{1}{N_b N_{\text{AF}}} \sum_{l=0}^{N_b-1} \sum_{n=1}^{N_{\text{AF}}} \mathbf{x}_{\text{st}}[nL_s + lN_t + N_s] \times \mathbf{x}_{\text{st}}^H[nL_s + lN_t + N_s] \tag{5}$$

where L_s is the number of sample points over which the length N_s window is slid in forming the new space-time snapshot after averaging in the current space-time snapshot, and $N_{\text{AF}} \leq \lfloor (N_t - 2N_s)/L_s \rfloor$ is the number of the snapshot extracted away from the "RAKE fingers."

[1]Note that this model allows multiple paths for each MUAI. For example, two multipaths from the same MUAI are viewed as two MUAI's having the same PN code but different timing offsets.

A. Asymptotic Structure of SOI and MUAI Space-Time Correlation Matrices

Assuming approximate bit synchronization for the desired user and the processing gain N_c to be large, the term in $\mathbf{x}_{\text{st}}[n]$ associated with the SOI is only non-negligible corresponding to the index $lN_t, l = 1, \ldots, N_b$. Denoting the SOI, MUAI, and noise contributions by the respective subscripts S, I, and N

$$\mathbf{x}_{\text{st}}[lN_t] \triangleq \mathbf{x}_{\text{RF}}[n] = \mathbf{x}_S[n] + \mathbf{x}_I[n] + \mathbf{x}_N[n] \quad l = 1, 2, \ldots, N_b \tag{6}$$

where $\mathbf{x}_{\text{RF}}[n]$ denotes the $MN_s \times 1$ space-time snapshot extracted from where the RAKE "fingers" lie. Employing a space-time RAKE receiver [3], the decision variable for the nth symbol is

$$z = z^{\text{st}} = \mathbf{w}^H \mathbf{x}_{\text{RF}}[n] \tag{7}$$

where $\mathbf{w}$ is an $MN_s \times 1$ space-time weight vector that combines the samples encompassing the RAKE fingers across both space and time, as depicted in Fig. 2.

Denote the asymptotic form of the $N \times N$ space-time correlation matrix of $\mathbf{x}_S[n], \mathbf{x}_I[n]$, and $\mathbf{x}_N[n]$ as $\mathbf{K}_S, \mathbf{K}_I$, and $\mathbf{K}_N$, respectively. Assuming statistical independence between and among the SOI, MUAI, and receiver noise components

$$\mathbf{K}_{S+I+N} = \mathbf{K}_S + \mathbf{K}_I + \mathbf{K}_N$$

where each of the matrices above is $N \times N$, with $N = MN_s$, where M is the number of antennas, and N_s is the number of (temporal) samples that encompass the multipath delay spread at each antenna, as depicted in Fig. 2.

Asymptotic Structure of $\mathbf{K}_S$: $\mathbf{x}_S[n]$ in (6) may be expressed as

$$\mathbf{x}_S[n] \triangleq \text{vec}(D(n)\mathbf{A}_S\mathbf{\Sigma}_S\mathbf{V}_S) \tag{8}$$

where vec( ) is an operator that maps an $M \times N_s$ matrix to an MN_s vector by concatenating its columns; $\mathbf{A}_S, \mathbf{\Sigma}_S$ and $\mathbf{V}_S$ are defined as follows. $\mathbf{A}_S = [\mathbf{a}(\theta_1), \ldots, \mathbf{a}(\theta_P,)]$ $(M \times P)$, $\mathbf{\Sigma}_S = N_c \,\text{diag}\{\rho_1, \ldots, \rho_P\}$, which is a $P \times P$ diagonal matrix containing the complex amplitudes of the P dominant multipaths for the SOI at the reference element, and each row of $\mathbf{V}_S$ is a sampled version of a time-delayed replica of $r_{cc}(\tau)$ delayed by τ_k, where k is the row index, i.e., we have (9), shown at the bottom of the next page, where $\mathbf{t}(\tau) = [r_{cc}(-\tau)\ r_{cc}((T_c/L_c)-\tau)\ \cdots\ r_{cc}((N_s-1)(T_c/L_c)-\tau)]^T$, and $r_{cc}(\tau)$ is the autocorrelation function for the SOI's spreading waveform $c(t)$. In the case where the chip waveform $p_c(t)$ is rectangular and the processing gain is large, $r_{cc}(\tau)$ approximately has the following triangular shape:

$$r_{cc}(\tau) = \begin{cases} 1 - \frac{|\tau|}{T_c}, & \text{if } |t| \leq T_c \\ 0, & \text{if } |t| > T_c. \end{cases} \tag{10}$$

Since the only random quantity in the SOI is $D(n)$, it follows that

$$\mathbf{K}_S = E\left[\mathbf{x}_S[n]\mathbf{x}_S^H[n]\right] = \sigma_b^2 \mathbf{d}\mathbf{d}^H \tag{11}$$

where $\sigma_b^2 = E[D^2(n)]$, and

$$\mathbf{d} = \text{vec}(\mathbf{A}_S \mathbf{\Sigma}_S \mathbf{V}_S) = N_c \sum_{k=1}^{P} \rho_k \mathbf{t}(\tau_k) \otimes \mathbf{a}\left(\theta_k^d\right) \tag{12}$$

which is the post-correlation space-time signature of the desired user that describes the gain and phase of each RAKE finger across space and time.

Asymptotic Structure of $\mathbf{K}_I$: The component of the $N \times 1$ space-time snapshot due to MUAI is

$$\mathbf{x}_I[n] \triangleq \text{vec}(\mathbf{A}_I \mathbf{\Sigma}_I \mathbf{D}_I(n) \mathbf{V}_I). \tag{13}$$

$\mathbf{\Sigma}_I$ is a $J \times J$ diagonal matrix containing the amplitudes (at the reference element) $\sigma_i, i = 1, \ldots, J$ for each of the MUAI's, and $\mathbf{D}_I(n)$ is a $J \times J$ diagonal matrix containing the bit values. The columns of the $M \times J$ matrix $\mathbf{A}_I$ are $\mathbf{a}(\theta_i), i = 1, \ldots, J$. The ith row of the $J \times N_s$ matrix $\mathbf{V}_I$ is the sequence matched filter output contributed from the ith interference. The MUAI space-time correlation matrix $\mathbf{K}_I = E[\mathbf{x}_I[n]\mathbf{x}_I^H[n]]$ may be expressed as

$$\mathbf{K}_I = \mathbf{R}_I \otimes \mathbf{A}_I \mathbf{\Sigma}_I^2 \mathbf{A}_I^H \tag{14}$$

where $\otimes$ is the Kronecker product, and we have exploited the following four properties:

i) $\text{vec}(\mathbf{ADB}) = (\mathbf{B}^T \otimes \mathbf{A})\,\text{vec}(\mathbf{D})$;
ii) $(\mathbf{A} \otimes \mathbf{B})(\mathbf{C} \otimes \mathbf{D}) = (\mathbf{AC}) \otimes (\mathbf{BD})$;
iii) data from different sources are assumed to be uncorrelated;
iv) $E[s_i(m)s_j(\ell)] = \delta_{ij}\delta_{m\ell}$, where the chip values comprising each PN sequence are modeled as independent and identically distributed.

$\mathbf{R}_I$ is a Toeplitz-symmetric matrix whose first column is $r_{cc}(mT_c/L_c)$, $m = 0, \ldots, N_s - 1$. Note that the $N_s \times N_s$ matrix $\mathbf{R}_I$ is full rank and that the $M \times J$ matrix $\mathbf{A}_I$ is rank J. It follows that $\mathbf{K}_I$ is rank $N_s J$.

Asymptotic Structure of $\mathbf{K}_N$: Denote $\mathbf{N}[n](M \times N_s)$ as the additive noise contribution; the rows of $\mathbf{N}[n]$ are independent Gaussian processes, but the individual components of each row are correlated because of the matched filtering operation. A similar development reveals that the space-time correlation matrix for $\mathbf{x}_N[n] \triangleq \text{vec}(\mathbf{N}[n])$ has the asymptotic form

$$\mathbf{K}_N = \mathbf{R}_N \otimes \mathbf{I}_N \tag{15}$$

where $\mathbf{R}_N$ is a Toeplitz-symmetric matrix whose first column is $r_{cc}(mT_c/L_c)$, $m = 0, \ldots, N_s - 1$.

Asymptotic Structure in Reduced Dimension: For later developments, the asymptotic expressions of a reduced-dimension matrix $\mathbf{A}^r$ and vector $\mathbf{d}^r$ related to the full-dimension counterparts $\mathbf{A}$ and $\mathbf{d}$ are formed as

$$\mathbf{A}^r = \mathbf{T}^{rH} \mathbf{A} \mathbf{T}^r, \quad \mathbf{d}^r = \mathbf{T}^{rH} \mathbf{d} \tag{16}$$

where $\mathbf{T}^r$ is a compression matrix, which we will provide criterion for design.

B. Relation to Space-Time MVDR Processing

We here show that the asymptotic space-time weight vector $\mathbf{w}$ obtained as the "largest" generalized eigenvector of the matrix pencil $\{\mathbf{K}_{S+I+N}, \mathbf{K}_{I+N}\}$ is the solution to the minimum variance distortionless response (MVDR) problem

$$\begin{aligned} &\min_{\mathbf{w}} \mathbf{w}^H \mathbf{K}_{I+N} \mathbf{w} \\ &\text{subject to: } \mathbf{w}^H \mathbf{d} = 1 \end{aligned} \tag{17}$$

where $\mathbf{d}$ is the $MN_s \times 1$ vector defined in (12). It is well known (and easily shown) that the solution to the above problem is $\mathbf{w}_{\text{MVDR}} = \alpha \mathbf{K}_{I+N}^{-1} \mathbf{d}$, where $\alpha = 1/\mathbf{d}^H \mathbf{K}_{I+N}^{-1} \mathbf{d}$.

The "largest" generalized eigenvector of the pencil $\{\mathbf{K}_{S+I+N}, \mathbf{K}_{I+N}\}$ is the solution to the unconstrained optimization problem

$$\begin{aligned} \max_{\mathbf{w}} \frac{\mathbf{w}^H \mathbf{K}_{S+I+N} \mathbf{w}}{\mathbf{w}^H \mathbf{K}_{I+N} \mathbf{w}} &= \max_{\mathbf{w}} \frac{\mathbf{w}^H \left(\mathbf{K}_{I+N} + \sigma_b^2 \mathbf{d}\mathbf{d}^H\right) \mathbf{w}}{\mathbf{w}^H \mathbf{K}_{I+N} \mathbf{w}} \\ &= \max_{\mathbf{w}} \frac{\mathbf{w}^H \mathbf{d}\mathbf{d}^H \mathbf{w}}{\mathbf{w}^H \mathbf{K}_{I+N} \mathbf{w}}. \end{aligned} \tag{18}$$

The transformation of variables defined by $\mathbf{z} = \mathbf{K}_{I+N}^{1/2} \mathbf{w}$, where $\mathbf{K}_{I+N}^{1/2}$ is the Hermitian spectral square root of $\mathbf{K}_{I+N}$, leads to the equivalent optimization problem

$$\max_{\mathbf{z}} \frac{\mathbf{z}^H \mathbf{K}_{I+N}^{-1/2} \mathbf{d}\mathbf{d}^H \mathbf{K}_{I+N}^{-1/2} \mathbf{z}}{\mathbf{z}^H \mathbf{z}}. \tag{19}$$

It follows immediately that the solution is $\mathbf{z} = \mathbf{K}_{I+N}^{-1/2} \mathbf{d}$ to within an inconsequential complex scalar multiple so that the optimal $\mathbf{w}$ is

$$\mathbf{w} = \mathbf{K}_{I+N}^{-1/2} \mathbf{z} = \mathbf{K}_{I+N}^{-1/2} \mathbf{K}_{I+N}^{-1/2} \mathbf{d} = \mathbf{K}_{I+N}^{-1} \mathbf{d} \tag{20}$$

which coincides with the solution to the space-time MVDR solution.

III. Reduced-Dimension Blind Space-Time 2-D RAKE Receiver

A reduced-dimension space-time RAKE receiver is obtained by restricting the space-time weight vector $\mathbf{w}$ to lie in a lower dimensional space spanned by the columns of the data-dependent

$$\mathbf{V}_S = \begin{bmatrix} \mathbf{t}^T(\tau_1) \\ \mathbf{t}^T(\tau_2) \\ \vdots \\ \mathbf{t}^T(\tau_P) \end{bmatrix} = \begin{bmatrix} r_{cc}(-\tau_1) & r_{cc}\left(\frac{T_c}{L_c} - \tau_1\right) & \cdots & r_{cc}\left((N_s - 1)\frac{T_c}{L_c} - \tau_1\right) \\ r_{cc}(-\tau_2) & r_{cc}\left(\frac{T_c}{L_c} - \tau_2\right) & \cdots & r_{cc}\left((N_s - 1)\frac{T_c}{L_c} - \tau_2\right) \\ \vdots & \vdots & \vdots & \vdots \\ r_{cc}(-\tau_P) & r_{cc}\left(\frac{T_c}{L_c} - \tau_P\right) & \cdots & r_{cc}\left((N_s - 1)\frac{T_c}{L_c} - \tau_P\right) \end{bmatrix} \tag{9}$$

dimensionality reducing matrix $\mathbf{T}^r$: $\mathbf{w} = \mathbf{T}^r\mathbf{w}_r$. The lower dimensional vector $\mathbf{w}_r$ is determined as the "largest" generalized eigenvector of the lower dimensional compressed matrix pencil $\{\mathbf{K}^r_{S+I+N}, \mathbf{K}^r_{I+N}\}$ according to

$$\underset{\mathbf{w}_r}{\text{Maximize}} \ \frac{\mathbf{w}_r^H \mathbf{K}^r_{S+I+N}\mathbf{w}_r}{\mathbf{w}_r^H \mathbf{K}^r_{I+N}\mathbf{w}_r}$$

where

$$\begin{aligned}\mathbf{K}^r_{S+I+N} &= \mathbf{T}^{rH}\mathbf{K}_{S+I+N}\mathbf{T}^r \\ \mathbf{K}^r_{I+N} &= \mathbf{T}^{rH}\mathbf{K}_{I+N}\mathbf{T}^r.\end{aligned} \tag{21}$$

The goal is to design $\mathbf{T}^r$ so that the largest generalized eigenvalue of the compressed matrix pencil $\{\mathbf{T}^{rH}\mathbf{K}_{S+I+N}\mathbf{T}^r, \mathbf{T}^{rH}\mathbf{K}_{I+N}\mathbf{T}^r\}$ is nearly equal to the largest generalized eigenvalue of the full-dimension space-time correlation matrix pencil $\{\mathbf{K}_{S+I+N}, \mathbf{K}_{I+N}\}$, which is equal to the asymptotic SINR.

The dimensionality reducing transformation matrix $\mathbf{T}^r$ is constructed as the Kronecker product of a temporal compression matrix $\mathbf{T}_C$ and a spatial compression matrix $\mathbf{T}_R$. $\mathbf{T}_C$ is based on a frequency domain implementation of a RAKE receiver. $\mathbf{T}_C$ is not dependent on the data and may be constructed *a priori* based on the chip waveform. $\mathbf{T}_R$ is a matrix beamformer that is data dependent based on the principal components of a spatial correlation matrix pencil. Applying both compressions sequentially yields the reduced-dimension beamspace-frequency matrix pencil. Despite the substantial reduction in dimensionality, there is a near negligible drop in asymptotic SINR as substantiated through analysis in Section IV. This implies faster convergence rate as well as lower computational complexity.

A. Temporal-Only Compression

The temporal transformation $\mathbf{T}_C$ transforms from a space of dimension equal to the number of taps needed to encompass the multipath delay spread to a lower dimensional frequency space. The $\mathbf{T}_C$ we propose is data independent based on a novel frequency domain implementation of a 1-D RAKE receiver [10]. With multiple antennas, the dimensionality reducing matrix is $\mathbf{T}^r = (\mathbf{T}_C \otimes \mathbf{I}_M)$.

1) Frequency Domain RAKE Receiver: To motivate the space-frequency implementation of a 2-D RAKE receiver, consider the case of a single antenna. Let $r_{yc}(t)$ denote the output of the matched filter based solely on spreading waveform of the desired user, i.e., the matched filter for the single path case. In the case of additive white noise prior to this filter, it is well known (and easily shown) that in the case of P dominant multipaths, the optimal (noncausal) decision statistic for making bit decisions is

$$z = \sum_{k=1}^{P} \rho_k^* r_{yc}(t+\tau_k)\Big|_{t=0} \tag{22}$$

where ρ_k and τ_k are the relative complex gain and time delay, respectively, of the kth multipath arrival. The initial value theorem and shift properties of the Fourier transform enable us to express the optimal decision statistic in the frequency domain as

$$\sum_{k=1}^{P} \rho_k^* r_{yc}(t+\tau_k)\Big|_{t=0} = \int_{-\infty}^{\infty} R_{yc}(f) \sum_{k=1}^{P} \rho_k^* e^{-j2\pi f\tau_k}\, df \tag{23}$$

where $R_{yc}(f)$ is the Fourier transform of $r_{yc}(t)$. Discretizing the integral, we have the approximation

$$\begin{aligned}&\sum_{k=1}^{P} \rho_k^* r_{yc}(t+\tau_k)\Big|_{t=0} \\ &\quad\approx \sum_{\ell=-L'}^{L'} R_{yc}(k\Delta f)\left\{\sum_{k=1}^{P} \rho_k^* e^{-j2\pi\ell\Delta f\tau_k}\right\}\Delta f.\end{aligned} \tag{24}$$

Thus, the optimal decision statistic may be expressed as a weighted sum of DFT values computed during the time window where the RAKE fingers occur, i.e.,

$$\sum_{k=1}^{P} \rho_k^* r_{yc}(t+\tau_k)\Big|_{t=0} \approx \mathbf{w}^H \mathbf{r}_{yc}^{(f)} \tag{25}$$

where $\mathbf{r}_{yc}^{(f)} = [R_{yc}(-L'\Delta f), \ldots, R_{yc}(0), \ldots, R_{yc}(L'\Delta f)]^T$ and

$$\mathbf{w} = \left[\sum_{k=1}^{P} \rho_k e^{-j2\pi L'\Delta f\tau_k}, \ldots, \sum_{k=1}^{P} \rho_k, \ldots, \sum_{k=1}^{P} \rho_k e^{j2\pi L'\Delta f\tau_k}\right]^T. \tag{26}$$

Since a beam is simply a weighted sum of antenna outputs, it follows that a 2-D RAKE receiver that optimally combines multipath while simultaneously cancelling interference in forming the decision statistic may be effected via one set of space-frequency weights that maximizes SINR. The optimal set of frequency weights depends on the relative amplitude, phase, and time delay of each multipath arrival. The goal here, however, is to blindly estimate the "best" weights without attempting to estimate these physical parameters.

Note that the space-time 2-D RAKE receiver is premised on the fact that the optimal decision statistic for a single antenna may be expressed as $z = \sum_{k=1}^{P} \rho_k^* r_{yc}(\tau_k)$ in accordance with (22). Thus, in a sampled setting, optimal performance of the space-time 2-D RAKE receiver requires sampling exactly at the multipath arrival times. Further, a blind time domain-based RAKE receiver should ideally work to set to zero those weight values corresponding to sample times in between the multipath arrival times in the case of a rectangular chip waveform. In contrast, the frequency domain RAKE receiver only requires that we sample greater than Nyquist and evaluate the spectrum at enough frequency points so that the sum on the right-hand side of (24) adequately approximates the integral on the right-hand side of (23).

The main advantage of a frequency domain implementation of a RAKE receiver is that we can select only those frequency values within the mainlobe of the spectrum of the autocorrelation function of the spreading waveform. Further, as will be substantiated by the simulations presented in Section VI, the number of such values required for "good" performance can be substantially less than the number of time samples

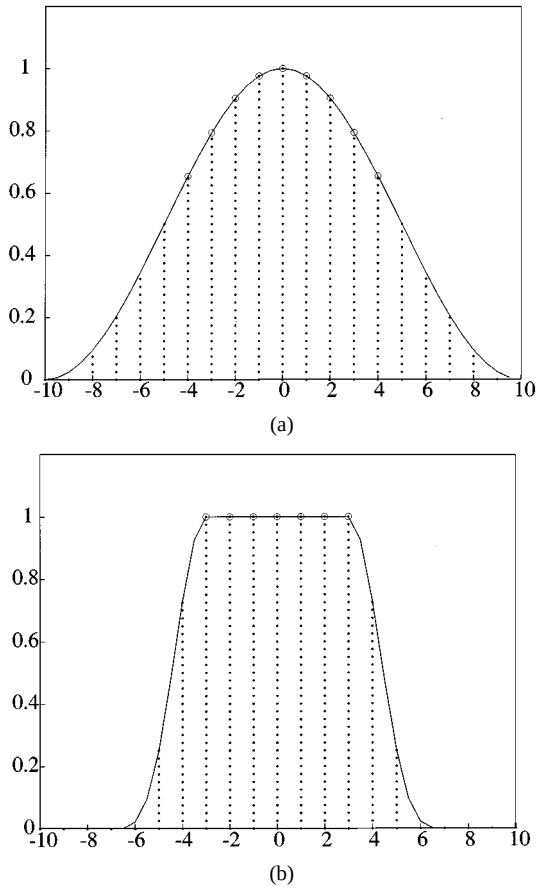

Fig. 1. Twenty-point DFT of the autocorrelation of the chip waveforms. (a) Square root raised cosine chip waveform, $\beta = 0.4$. (b) Rectangular chip waveform.

recorded during the multipath time delay spread. The result is that the space-frequency correlation matrix pencil can be of significantly smaller dimension than the space-time correlation matrix pencil with little degradation in performance.

2) Blind Space-Frequency 2-D RAKE Receiver: The processing scheme constituting the blind space-frequency 2-D RAKE receiver [10] is similar to Fig. 2, except it only does the temporal compression using frequency samples with no spatial compression. Assuming approximate synchronization information on the desired user, K_C values of the Fourier transform of the 10-μs (or so) time window containing the fingers are computed. The K_C spectral values from each of the M antennas for a given bit are stacked in an $MK_C \times 1$ column vector. The $MK_C \times MK_C$ signal plus interference (plus noise) space-frequency matrix, which is denoted $\mathbf{K}^{\rm sf}_{S+I+N}$, is then formed as the outer product of this vector with itself incoherently averaged over a number of bits for which the multipath environment is relatively stationary.

The $MK_C \times MK_C$ interference only (plus noise) space-frequency matrix, which is denoted $\mathbf{K}^{\rm sf}_{I+N}$, is estimated similarly over the remaining portion of the bit period. Since the fingers occupy only a fraction of the bit period, $\hat{\mathbf{K}}^{\rm sf}_{I+N}$ is formed by incoherently averaging over multiple $MK_C \times 1$ snapshots extracted from a single bit period, as well as by averaging over $MK_C \times 1$ snapshots extracted from adjacent bit periods during which the multipath scenario stays relatively constant. The optimum weight vector for combining the K_C spectral values computed in the vicinity of the fingers for each of the M antennas is the "largest" generalized eigenvector of the $MK_C \times MK_C$ matrix pencil $\{\hat{\mathbf{K}}^{\rm sf}_{S+I+N}, \hat{\mathbf{K}}^{\rm sf}_{I+N}\}$.

3) Asymptotic SINR with Temporal-Only Compression: We take only $K_C < N_s$ frequency samples containing the most energy that are selected, as shown in Fig. 1 for the cases of rectangular and spectral square-root raised cosine chip waveforms. In this case, without invoking spatial compression, the dimensionality reducing matrix is $\mathbf{T}^r = (\mathbf{T}_C \otimes \mathbf{I}_M)$, where $\mathbf{T}^*_C$ is simply K_C columns of the N_s pt. DFT matrix. Dimensionality reduction is achieved by exploiting the simple fact that most of the energy of the desired user is contained in the lower frequency samples near DC. For example, if the delay spread is 10 μs, the time between chips is 1 μs, and we sample two times per chip, 20 time samples encompass the multipath spread. In this case, simulations have revealed that $\mathbf{T}_C$ is simply nine columns of the 20-point DFT matrix, which results in good performance. Therefore, the criterion for finding space-frequency weight vector that maximize SINR is equivalent to

$$\begin{aligned} &\underset{\mathbf{w}_{\rm sf}}{\text{Maximize}} \ \frac{\mathbf{w}^H_{\rm sf}\mathbf{K}^{\rm sf}_{S+I+N}\mathbf{w}_{\rm sf}}{\mathbf{w}^H_{\rm sf}\mathbf{K}^{\rm sf}_{I+N}\mathbf{w}_{\rm sf}} \\ &\quad \equiv \underset{\mathbf{w}_{\rm sf}}{\text{Maximize}} \ \frac{\mathbf{w}^H_{\rm sf}\mathbf{T}^{rH}\mathbf{K}_{S+I+N}\mathbf{T}\mathbf{w}_{\rm sf}}{\mathbf{w}^H_{r}\mathbf{T}^{rH}\mathbf{K}_{I+N}\mathbf{T}^{r}\mathbf{w}_{\rm sf}}. \end{aligned} \tag{27}$$

In the reduced dimension space-time RAKE receiver, where a dimensionality reducing transformation is applied only in the time dimension based on a frequency domain RAKE receiver as motivated in Section III-C1, the decision variable is

$$z^{\rm sf} = \hat{\mathbf{w}}^H_{\rm sf}\{(\mathbf{T}_C \otimes \mathbf{I}_M)^H \mathbf{x}_{\rm RF}[n]\}. \tag{28}$$

4) Analysis of Blind Cancellation of MUAI's: Here, we analyze how the reduced-dimension space-frequency RAKE receiver cancels strong MUAI's. We now prove that each $M \times 1$ subvector of the optimum weight vector corresponding to the spatial weights for a particular frequency bin is orthogonal to each column of $\mathbf{A}_I$. This is a result of the fact that each MUAI is a broadband interferer, thereby requiring a spatial null at each frequency bin to cancel it. This motivates the development of the spatial preprocessing scheme in the form of the reduced-dimension beamspace processing. This point will be addressed later.

Equation (14) reveals that the space-frequency correlation matrix of the MUAI is a Kronecker product of the $K_C \times K_C$ matrix $\mathbf{S}_F = \mathbf{T}^H_C\mathbf{R}_I\mathbf{T}_C$ with the $M \times M$ matrix $\mathbf{A}_I\mathbf{\Sigma}^2_I\mathbf{A}^H_I$, where K_C = number of selcted frequency bins. Let $\mathbf{E}_F$ be a $K_C \times K_C$ matrix whose columns are the eigenvectors of $\mathbf{S}_F$. Since $\mathbf{S}_F$ is a full-rank Hermitian matrix, it follows that $\mathbf{E}^H_F\mathbf{E}_F = \mathbf{E}_F\mathbf{E}^H_F = \mathbf{I}_{K_C}$. In contrast, $\mathbf{A}_I\mathbf{\Sigma}^2_I\mathbf{A}^H_I$ is only rank J, where J is the number of MUAI's. Let $\mathbf{E}_S$ be an $M \times J$ matrix whose columns are the eigenvectors of $\mathbf{A}_I\mathbf{\Sigma}^2_I\mathbf{A}^H_I$ associated with the J nonzero eigenvalues. From signal subspace theory, it follows that $\mathbf{E}_S = \mathbf{A}_I\mathbf{Q}$, where $\mathbf{Q}$ is a $J \times J$ full-rank matrix. Now, it was noted previously that $\mathbf{K}_I$ is of rank JK_C. Let $\mathbf{E}_I$ be an $MK_C \times JK_C$ matrix whose columns are the eigenvectors of $\mathbf{K}_I$ associated with the JK_C nonzero eigenvalues. It follows from the theory of Kronecker products that $\mathbf{E}_I = \mathbf{E}_F \otimes \mathbf{E}_S$.

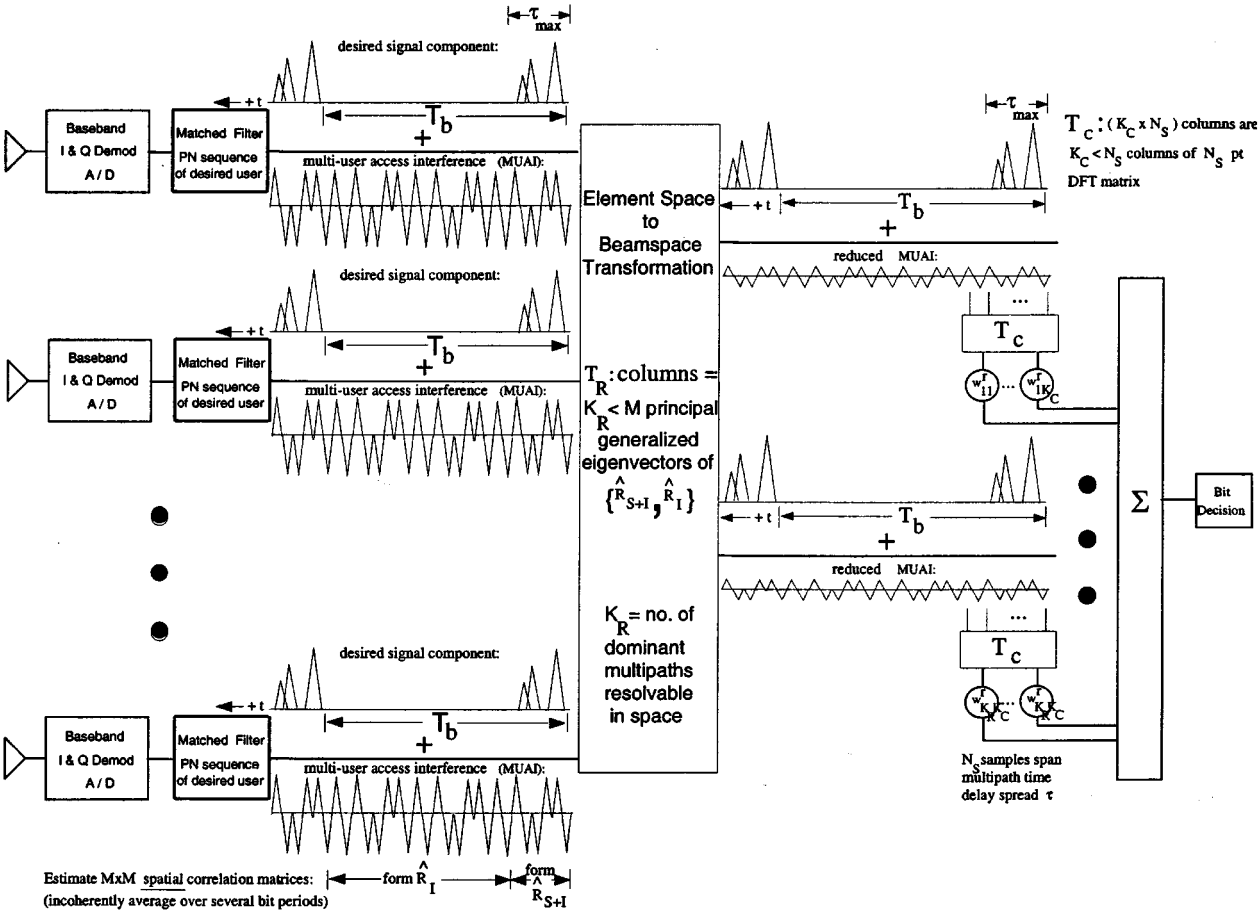

Fig. 2. Blind reduced dimension space-time 2-D RAKE receiver.

Postmultiplying $\mathbf{E}_I$ by a full-rank $JK_C \times JK_C$ matrix yields a matrix whose range space is the same as that of $\mathbf{E}_I$. Postmultiplying $\mathbf{E}_I$ by the full-rank matrix $\mathbf{E}_F^H \otimes \mathbf{Q}^{-1}$ yields

$$\mathbf{G}_I = \mathbf{E}_I \left(\mathbf{E}_F^H \otimes \mathbf{Q}^{-1}\right) = (\mathbf{E}_F \otimes \mathbf{E}_S)\left(\mathbf{E}_F^H \otimes \mathbf{Q}^{-1}\right) \quad (29)$$

$$= \mathbf{E}_F \mathbf{E}_F^H \otimes \mathbf{E}_S \mathbf{Q}^{-1} = \mathbf{I}_{K_C} \otimes \mathbf{A}_I \quad (30)$$

where we have used the Kronecker product property $(\mathbf{A} \otimes \mathbf{B})(\mathbf{C} \otimes \mathbf{D}) = (\mathbf{AC}) \otimes (\mathbf{BD})$. The projection operator $\mathbf{P}_I$ onto the range space of $\mathbf{K}_I$ may thus be expressed as

$$\mathbf{P}_I = \mathbf{E}_I \mathbf{E}_I^H = \mathbf{G}_I \left(\mathbf{G}_I^H \mathbf{G}_I\right)^{-1} \mathbf{G}_I^H = \mathbf{I}_{K_C} \otimes \mathbf{P}_{A_I} \quad (31)$$

where $\mathbf{P}_{A_I}$ is the $M \times M$ projection operator onto the subspace spanned by the columns of $\mathbf{A}_I$. To arrive at the final form of $\mathbf{P}_I$ on the far right-hand side of (31), we have used the additional Kronecker product properties $(\mathbf{A} \otimes \mathbf{B})^H = \mathbf{A}^H \otimes \mathbf{B}^H$ and $(\mathbf{A} \otimes \mathbf{B})^{-1} = \mathbf{A}^{-1} \otimes \mathbf{B}^{-1}$. It will be shown that the "largest" generalized eigenvector of the matrix pencil $\{\mathbf{K}_{S+I+N}^{\mathrm{sf}}, \mathbf{K}_{I+N}^{\mathrm{sf}}\}$ is the solution to the MVDR problem in (17). Consider the case where the power of the MUAI's is much stronger than the receiver generated noise such that $\mathbf{K}_{I+N}^{\mathrm{sf}} = \mathbf{K}_I^{\mathrm{sf}} + \mathbf{K}_N^{\mathrm{sf}} \approx \mathbf{K}_I^{\mathrm{sf}}$. Substituting this approximation into (17) yields

$$\min_{\mathbf{w}} \mathbf{w}^H \mathbf{K}_I^{\mathrm{sf}} \mathbf{w}$$

$$\text{subject to: } \mathbf{w}^H \mathbf{d}^{\mathrm{sf}} = 1 \quad (32)$$

where $\mathbf{d}^{\mathrm{sf}} = (\mathbf{T}_C \otimes \mathbf{I}_M)^H \mathbf{d}$ with the $MN_s \times 1$ vector $\mathbf{d}$ defined in (12). If the number of MUAI's J is less than the number of antennas M, $\mathbf{K}_I^{\mathrm{sf}}$ is rank $JK_C < MK_C$, as discussed previously. In this case, it is possible to make the objective function zero, which is the smallest possible value implying perfect cancellation of MUAI's, with $\mathbf{w}_{\mathrm{opt}} \approx \alpha(\mathbf{d}^{\mathrm{sf}} - \mathbf{P}_I \mathbf{d}^{\mathrm{sf}})$, where $\mathbf{P}_I$ is the projection operator onto the range space of $\mathbf{K}_I$ given by (31) and $\alpha = 1/\{(\mathbf{d}^{\mathrm{sf}} - \mathbf{P}_I \mathbf{d}^{\mathrm{sf}})^H \mathbf{K}_I^{\mathrm{sf}} (\mathbf{d}^{\mathrm{sf}} - \mathbf{P}_I \mathbf{d}^{\mathrm{sf}})\}$. Substituting the expression for $\mathbf{P}_I$ in (31) in $\mathbf{d}^{\mathrm{sf}} - \mathbf{P}_I \mathbf{d}^{\mathrm{sf}}$ yields the following asymptotic expression for the optimum weight vector:

$$\mathbf{w}_{\mathrm{opt}} = \alpha \begin{bmatrix} \mathbf{d}_1^{\mathrm{sf}} - \mathbf{P}_{AI} \mathbf{d}_1^{\mathrm{sf}} \\ \vdots \\ \mathbf{d}_{K_C}^{\mathrm{sf}} - \mathbf{P}_{AI} \mathbf{d}_{K_C}^{\mathrm{sf}} \end{bmatrix} \quad (33)$$

where $\mathbf{d}_i^{\mathrm{sf}}$ is the ith $M \times 1$ (nonoverlapping) subvector of the $MK_C \times 1$ vector $\mathbf{d}^{\mathrm{sf}}$. It follows that the ith $M \times 1$ subvector of $\mathbf{w}_{\mathrm{opt}}$ is orthogonal to each column of $\mathbf{A}_I$, i.e., the array pattern obtained at *each* frequency bin exhibits a spatial null in the direction of *each* and every MUAI.

B. Spatial Compression

Further compression may be achieved by exploiting cases where the angular spread of the desired user's multipath is a couple of the beamwidths of the antenna array. The data-dependent spatial transformation $\mathbf{T}_R$ transforms from element space to a lower dimensional beamspace. The beams formed from the columns of $\mathbf{T}_R$ ideally have mainlobes that encompass the angular spread of the desired user's multipath and nulls toward

each strong multiuser access interferer. This is effected blindly without direction finding as follows [9].

1) Blind Beamspace-Frequency 2-D RAKE Receiver: Spatial preprocessing is proposed to convert to a lower dimensional beamspace [9], prior to space-frequency processing, as illustrated in Fig. 2. In this scheme, we first transform to a $K_R < M$-dimensional subspace (beamspace) prior to space-frequency processing so that $\hat{\mathbf{K}}^r_{S+I+N}$ and $\hat{\mathbf{K}}^r_{I+N}$ are $K_RK_C \times K_RK_C$ as opposed to $MK_C \times MK_R$, where K_R depends on the angular spread of the multipath for the desired user in terms of beamwidths.

As shown in Fig. 2, the $M \times M$ *spatial* correlation matrix $\hat{\mathbf{R}}_{S+I+N}$ is formed from snapshots measured in the vicinity of the "fingers," whereas $\hat{\mathbf{R}}_{I+N}$ is formed from snapshots measured away from the "fingers." Note that a number of snapshots may be extracted from a single bit period for the purpose of forming $\hat{\mathbf{R}}_{S+I+N}$. For example, if the sampling rate is two times per chip and the multipath time delay spread is 10 μs, a single bit gives rise to 20 snapshots that may be incoherently averaged to form $\hat{\mathbf{R}}_{S+I+N}$. In contrast, only one snapshot per bit is available to form $\hat{\mathbf{K}}_{S+I+N}$. Thus, it takes a smaller number of bits to obtain a "good" estimate of $\hat{\mathbf{R}}_{S+I+N}$ relative to $\hat{\mathbf{K}}_{S+I+N}$.

The idea is based on employing the $K_R < M$ principal generalized eigenvectors of the matrix pencil $\{\hat{\mathbf{R}}_{S+I+N}, \hat{\mathbf{R}}_{I+N}\}$ as a set of beamforming weight vectors to transform the data from M-dimensional element space to a K_R-dimensional beamspace. *Each* of the K_R beams ideally has a null in the direction of each MUAI and substantial gain in the direction of one or more of the multipath arrivals associated with the desired user. The size of the beamspace K_R depends on the number of dominant multipaths resolvable in space. For example, if a second dominant multipath arrives angularly separated by more than a half-beamwidth and time-delayed more than a half chip (so that it is at least partially decorrelated) relative to the first multipath, the matrix pencil $\{\hat{\mathbf{R}}_{S+I+N}, \hat{\mathbf{R}}_{I+N}\}$ will have two principal generalized eigenvalues. The corresponding two principal generalized eigenvectors are employed to transform from M-dimensional element space to a 2-D beamspace to which the space-frequency processing scheme may be applied. Note that K_R may be as small as 1 if the angular spread of desired signal at base is small relative to beamwidth. A point spatial null will be put in the direction of each strong narrowband interferer if they are angularly separated by more than a beamwidth, thereby reducing the number of degrees of freedom in this scheme. However, if we restrict our attention to a scenario where the MUAI's are the primary source of interference, canceling each broadband MUAI consumes K_C degrees of freedom anyhow; therefore, J spatial nulls are formed toward the MUAI's at each of the K_C frequency bins, as shown in the analysis in Section III-A4. Thus, the interference rejection capability of the scheme is not lessened under this separable processing approach.

2) Two-Stage Processing Transformations: With the blind spatial preprocessing scheme, we first estimate the spatial-only matrix pencil $\{\hat{\mathbf{R}}_{S+I+N}, \hat{\mathbf{R}}_{I+N}\}$ and then calculate its K_R "largest" generalized eigenvectors to form the the beamspace compression matrix $\mathbf{T}_R$. We then apply the beamspace-frequency processing scheme. Alternatively, we may form the full-dimension space-time matrix pencil $\{\hat{\mathbf{K}}_{S+I+N}, \hat{\mathbf{K}}_{I+N}\}$ and construct the lower dimensional compressed matrix pencil $\{\hat{\mathbf{K}}^r_{S+I+N}, \hat{\mathbf{K}}^r_{I+N}\}$ through the following relations. We are able to calculate $\{\hat{\mathbf{R}}_{S+I+N}, \hat{\mathbf{R}}_{I+N}\}$ from the space-time matrix pencil $\{\hat{\mathbf{K}}_{S+I+N}, \hat{\mathbf{K}}_{I+N}\}$ via

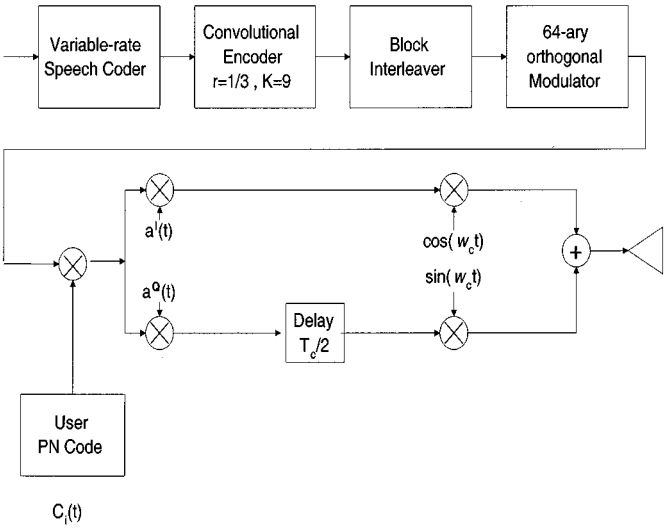

Fig. 3. IS-95 transmitter structure for the uplink.

$$\hat{\mathbf{R}}_{S+I+N} = \frac{1}{N_s}\sum_{l=0}^{N_s-1} \mathbf{\Gamma}_l^T \hat{\mathbf{K}}_{S+I+N}\mathbf{\Gamma}_l;$$
$$\hat{\mathbf{R}}_{I+N} = \frac{1}{N_s}\sum_{l=0}^{N_s-1} \mathbf{\Gamma}_l^T \hat{\mathbf{K}}_{I+N}\mathbf{\Gamma}_l \tag{34}$$

where the $MN_s \times M$ matrix

$$\mathbf{\Gamma}_l = \begin{bmatrix} \mathbf{0} \\ \mathbf{I}_M \\ \mathbf{0} \end{bmatrix} \begin{matrix} (l-1)M \\ M \\ (N_s - l)M. \end{matrix}$$

The columns of the spatial compression matrix $\mathbf{T}_R(M \times K_R)$ are formed by the K_R "largest" generalized eigenvectors of $\{\hat{\mathbf{R}}_{S+I+N}, \hat{\mathbf{R}}_{I+N}\}$. It follows that the $K_RK_C \times 1$ beamspace-frequency weights $\mathbf{w}_r$ are computed as the "largest" generalized eigenvector of the $K_RK_C \times K_RK_C$ matrix pencil $\{\hat{\mathbf{K}}^r_{S+I+N}, \hat{\mathbf{K}}^r_{I+N}\}$, where

$$\hat{\mathbf{K}}^r_{S+I+N} = (\mathbf{T}_C \otimes \mathbf{T}_R)^H \hat{\mathbf{K}}_{S+I+N}(\mathbf{T}_C \otimes \mathbf{T}_R)$$
$$\hat{\mathbf{K}}^r_{I+N} = (\mathbf{T}_C \otimes \mathbf{T}_R)^H \hat{\mathbf{K}}_{I+N}(\mathbf{T}_C \otimes \mathbf{T}_R). \tag{35}$$

In the reduced-dimension space-time RAKE receiver, where dimensionality reducing transformations are applied sequentially in both the space and time dimensions as shown in Fig. 3, the decision variable is

$$z^r = \hat{\mathbf{w}}_r^H \{(\mathbf{T}_C \otimes \mathbf{T}_R)^H \mathbf{x}_{\mathrm{RF}}[n]\} \tag{36}$$

IV. Asymptotic SINR and Convergence Analysis

A. Asymptotic SINR Analysis

The section will provide an analysis of the loss in asymptotic SINR incurred with reduced dimension processing. Asymptot-

ically, $\mathbf{K}_{S+I+N} = \sigma_s^2 \mathbf{d}\mathbf{d}^H + \mathbf{K}_{I+N}$. For the full- and reduced-dimension cases, respectively, it is easy to show that

$$\begin{aligned}\text{SINR}_{\text{opt}} &= \underset{\mathbf{w}}{\text{Maximize}}\ \frac{\mathbf{w}^H \mathbf{K}_{S+I+N}\mathbf{w}}{\mathbf{w}^H \mathbf{K}_{I+N}\mathbf{w}} - 1 \\ &= \mathbf{d}^H \mathbf{K}_{I+N}^{-1}\mathbf{d}, \quad \text{when } \mathbf{w} = \mathbf{w}_{\text{opt}} \propto \mathbf{K}_{I+N}^{-1}\mathbf{d}\end{aligned} \tag{37}$$

$$\begin{aligned}\text{SINR}_{\text{opt}}^r &= \underset{\mathbf{w}^r}{\text{Maximize}}\ \frac{\mathbf{w}^{rH} \mathbf{K}_{S+I+N}^r \mathbf{w}^r}{\mathbf{w}^{rH} \mathbf{K}_{I+N}^r \mathbf{w}^r} - 1 \\ &= \mathbf{d}^{rH} \left\{\mathbf{K}_{I+N}^r\right\}^{-1} \mathbf{d}^r, \\ &\qquad \text{when } \mathbf{w}^r = \mathbf{w}_{\text{opt}}^r \propto \left\{\mathbf{K}_{I+N}^r\right\}^{-1} \mathbf{d}^r\end{aligned} \tag{38}$$

where $\mathbf{d}^r = \mathbf{T}^{rH}\mathbf{d}$. To quantify the loss in asymptotic SINR, we define the following matrixes:

$$\begin{aligned}\mathbf{T}^H \mathbf{K}_{I+N}\mathbf{T} &= \begin{bmatrix} \mathbf{K}_{I+N}^r & \mathbf{K}_{12} \\ \mathbf{K}_{21} & \mathbf{K}_{22}\end{bmatrix} \\ &= \begin{bmatrix} \mathbf{T}^{rH}\mathbf{K}_{I+N}\mathbf{T}^r & \mathbf{T}^{rH}\mathbf{K}_{I+N}\mathbf{T}^c \\ \mathbf{T}^{cH}\mathbf{K}_{I+N}\mathbf{T}^r & \mathbf{T}^{cH}\mathbf{K}_{I+N}\mathbf{T}^c\end{bmatrix}\end{aligned} \tag{39}$$

where $\mathbf{T} = [\mathbf{T}^r \vdots \mathbf{T}^c]$, and $\mathbf{T}^c$ is an $N \times (N - N^r)$ matrix whose columns span the orthogonal complement of the range space of $\mathbf{T}^r$. After some algebraic manipulations, we have

$$\begin{aligned}\text{SINR}_{\text{opt}} = \text{SINR}_{\text{opt}}^r &+ \left(\mathbf{d}^c - \mathbf{K}_{21}\left\{\mathbf{K}_{I+N}^r\right\}^{-1}\mathbf{d}^r\right)^H \\ &\times \left\{\mathbf{K}_{22} - \mathbf{K}_{21}^H \left\{\mathbf{K}_{I+N}^r\right\}^{-1}\mathbf{K}_{12}\right\}^{-1} \\ &\times \left(\mathbf{d}^c - \mathbf{K}_{21}\left\{\mathbf{K}_{I+N}^r\right\}^{-1}\mathbf{d}^r\right)\end{aligned} \tag{40}$$

where $\mathbf{d}^c = \mathbf{T}^{cH}\mathbf{d}$. It can be shown that the second quantity on the right-hand side of (40) is non-negative so that $\text{SINR}_{\text{opt}} \geq \text{SINR}_{\text{opt}}^r$. This analysis serves to quantify the loss in asymptotic SINR incurred with a particular compression matrix $\mathbf{T}^r$. Empirically, the loss incurred in each simulation example was determined to be less than 1.5 dB.

B. Convergence: Space-Time versus Reduced-Dimension Beamspace-Frequency

Assume that we have averaged over enough space-time snapshots to average out the cross-terms between desired signal and either MUAI or noise. In this case, $\hat{\mathbf{K}}_{S+I+N} = \hat{\sigma}_s^2 \mathbf{d}\mathbf{d}^H + \hat{\hat{\mathbf{K}}}_{I+N}$, where $\hat{\hat{\mathbf{K}}}_{I+N}$ arises from the contribution of MUAI and noise to the RAKE fingers; $\hat{\hat{\mathbf{K}}}_{I+N}$ is an estimate of $\mathbf{K}_{I+N}$ but averaged over a fraction of the number of snapshots (one per bit) used to form $\hat{\mathbf{K}}_{I+N}$, which, recall, is averaged over the many space-time snapshots extracted away from the "RAKE fingers." Thus, we have

$$\begin{aligned}\widehat{\text{SINR}}_{\text{opt}} &= \underset{\mathbf{w}}{\text{Maximize}}\ \frac{\mathbf{w}^H \hat{\mathbf{K}}_{S+I+N}\mathbf{w}}{\mathbf{w}^H \hat{\mathbf{K}}_{I+N}\mathbf{w}} - 1 \\ &= \underset{\mathbf{w}}{\text{Maximize}} \left\{\frac{\mathbf{w}^H \left(\hat{\sigma}_s^2 \mathbf{d}\mathbf{d}^H\right)\mathbf{w}}{\mathbf{w}^H \hat{\mathbf{K}}_{I+N}\mathbf{w}} \right. \\ &\qquad \left. + \frac{\mathbf{w}^H \hat{\hat{\mathbf{K}}}_{I+N}\mathbf{w}}{\mathbf{w}^H \hat{\mathbf{K}}_{I+N}\mathbf{w}} - 1\right\}\end{aligned}$$

where $\widehat{\text{SINR}}_{\text{opt}}$ is the optimum SINR achieved in the practical case of a finite number of space-time snapshots N_{ss}. The expected value of $\{(\mathbf{w}^H \hat{\hat{\mathbf{K}}}_{I+N}\mathbf{w}/\mathbf{w}^H \hat{\mathbf{K}}_{I+N}\mathbf{w}) - 1\}$ is small compared with the first term. We thus concentrate on the first term $(\mathbf{w}^H(\hat{\sigma}_s^2 \mathbf{d}\mathbf{d}^H)\mathbf{w}/\mathbf{w}^H \hat{\mathbf{K}}_{I+N}\mathbf{w})$ in the expression on the far right-hand side above. Assuming the number of space-time snapshots for estimating $\hat{\mathbf{K}}_{I+N}$, N_{ss}, to be larger than the full-dimension N, which is the size of $\mathbf{K}_{S+I+N}$ and $\mathbf{K}_{I+N}$, and therefore larger than the reduced dimension N^r, which is the size of $\mathbf{K}_{S+I+N}^r$ and $\mathbf{K}_{I+N}^r$, the theory developed in [14] for MVDR processing may be utilized to prove

$$\begin{aligned}E[\widehat{\text{SINR}}_{\text{opt}}] &\approx \left(\frac{N_{\text{ss}} - N + 3}{N_{\text{ss}} + 2}\right) \text{SINR}_{\text{opt}} \\ E[\widehat{\text{SINR}}_{\text{opt}}^r] &\approx \left(\frac{N_{\text{ss}} - N^r + 3}{N_{\text{ss}} + 2}\right) \text{SINR}_{\text{opt}}^r.\end{aligned} \tag{41}$$

The optimal weight vector $\mathbf{w}$ is approximated by $\hat{\mathbf{K}}_{I+N}^{-1}\mathbf{d}$ for deriving the result (41). Note that the snapshots are assumed to be i.i.d. Gaussian vectors with zero mean in the derivation of the expression (41). However, sliding the time window to extract multiple overlapped snapshots in the algorithms can improve the performance. Since $N^r < N$ and $\text{SINR}_{\text{opt}}^r \approx \text{SINR}_{\text{opt}}$, it follows that

$$E\left[\widehat{\text{SINR}}_{\text{opt}}^r\right] > E[\widehat{\text{SINR}}_{\text{opt}}]. \tag{42}$$

Thus, in addition to leading to reduced computational complexity, reduced-dimension processing leads to a higher output SINR in the practical case of a finite number of space-time snapshots.

V. Adaptation to the IS-95 Uplink

A. Space-Time Data Model for the IS-95 Uplink

The transmitter block diagram for the uplink of IS-95 is shown in Fig. 3 [11]. Two information bits are mapped to six bits via a rate $1/3$ convolutional encoder. These six bits are grouped together as an index to select one of 64 Walsh–Hadamard functions, which is then subsequently multiplied by a (time-varying) user's spreading waveform $c_i(t)$ with four chips per "Walsh" chip. Note that the period of $c_i(t)$ is $2^{42} - 1$. The data is further spread by two short codes $a^I(t)$ and $a^Q(t)$ with period equal to 2^{15} to create the I and Q channels, respectively. The resulting I and Q channels, which carry the same information bits, are then input to an offset-QPSK modulator with the Q channel signal delayed by a half chip period $T_c/2$, relative to the I channel signal.

The jth symbol transmitted by the ith user is described as

$$\begin{aligned}\mathbf{s}_i(t) = &\sqrt{P_i} W_i^j(t) a_i^{\mathbf{I}}(t)\cos(\omega_c t) \\ &+ \sqrt{P_i} W_i^j\left(t - \frac{T_c}{2}\right) a_i^{\mathbf{Q}}\left(t - \frac{T_c}{2}\right)\sin(\omega_c t) \\ &\qquad 0 \leq t \leq T_w.\end{aligned} \tag{43}$$

The various quantities in (43) are described below. We define $W_i^j(t)$ as the Walsh symbol, and j is referred to as the Walsh function index: $j = 1, 2, \ldots, 64$. P_i is the transmitted power per symbol. ω_c is the carrier frequency in radians. T_w is the duration of a Walsh symbol. $a_i^I(t)$ and $a_i^Q(t)$ are the PN spreading codes applied to the I and Q channels, respectively:

$$a_i^I(t) = c_i(t)a^I(t) \quad a_i^Q(t) = c_i(t)a^Q(t).$$

Denoting the chip waveform as $p(t)$

$$a_i^I(t) = \sum_{n=-\infty}^{\infty} a_{i,n}^I p(t - nT_c)$$
$$a_i^Q(t) = \sum_{n=-\infty}^{\infty} a_{i,n}^Q p(t - nT_c) \quad (44)$$

where $a_{i,n}^I$ and $a_{i,n}^Q$ are distinct PN sequences.

The baseband representation of the $M \times 1$ array snapshot vector $\mathbf{x}(t)$ containing the outputs of each of the M antennas comprising the array at time t is modeled as

$$\begin{aligned}\mathbf{x}(t) = &\sum_{k=1}^{P_d} \rho_{d,k}\mathbf{a}\left(\theta_k^d\right)\left[W_d^j(t-\tau_{d,k})a_d^{\mathbf{I}}(t-\tau_{d,k})\right.\\ &\left. + jW_d^j\left(t-\frac{T_c}{2}-\tau_{d,k}\right)a_d^{\mathbf{Q}}\left(t-\frac{T_c}{2}-\tau_{d,k}\right)\right]\\ &+\sum_{i=1}^{J}\sum_{k=1}^{P_i}\rho_{i,k}\mathbf{a}\left(\theta_k^i\right)\left[W_i^j(t-\tau_{i,k})a_i^{\mathbf{I}}(t-\tau_{i,k})\right.\\ &\left. + jW_i^j\left(t-\frac{T_c}{2}-\tau_{i,k}\right)a_i^{\mathbf{Q}}\left(t-\frac{T_c}{2}-\tau_{i,k}\right)\right]\\ &+\mathbf{n}_w(t)\end{aligned}$$

where d denotes the desired user. $\mathbf{a}(\theta)$ is the spatial response of the array. For a given user i

- P_i number of different paths from which the ith signal arrives;
- θ_k^i arrival direction of the kth multipath;
- $\tau_{i,k}$ corresponding relative delay of the kth multipath;
- $\rho_{i,k}$ complex amplitude of the kth multipath arrival for the ith signal at the reference element.

J MUAI's impinge on the array. The vector $\mathbf{n}_w(t)$ represents the contribution of bandlimited noise.

B. 2-D RAKE Receiver for IS-95 Uplink

The IS-95 uplink is a noncoherent modulation scheme employing time-varying spreading waveforms and 64-ary orthogonal signaling based on Walsh functions. One Walsh symbol period is 208.33 μs; the chip rate is 1.2288 Mchips/s. In contrast to the BPSK modulation and time-invariant spreading assumed in classical DS-CDMA, we now have to sift through 64 outputs from a matched filter bank to determine which Walsh symbol was sent, as opposed to one matched filter in the BPSK case. To adapt our previous two-stage blind 2-D RAKE receiver for the IS-95 uplink, we assume that a small sequence (3–5 Walsh symbols) is available through some initialization stage at the front end of a transmission burst[2] and then move into a decision directed mode of operation. The respective indexes of several preceding Walsh symbol decisions tells us which matched filter outputs contain the fingers so that we can estimate $\mathbf{R}_{S+I+N}$ and $\mathbf{R}_{I+N}$ ($\mathbf{K}_{S+I+N}^r$ and $\mathbf{K}_{I+N}^r$) by incoherently averaging over the appropriate space (beamspace-frequency) snapshots extracted from several successive Walsh symbol periods. After downconverting to baseband, the output of each antenna is put through a matched filter bank that is essentially the reverse of the operations depicted in the transmitter block diagram in Fig. 3 (omitting the coding and interleaver blocks) but one for each of the 64 possible Walsh symbols. The matched filters comprising the bank are

$$\begin{aligned}h^j(t;m) = &W^j(T_w - t)a_d^{\mathbf{I}}(T_w - t + mT_w)\\ &- jW^j\left(T_w - t + \frac{T_c}{2}\right)\\ &\times a_d^{\mathbf{Q}}\left(T_w - t + \frac{T_c}{2} + mT_w\right)\\ &0 \le t \le T_w, \quad j = 1, 2, \ldots, 64\end{aligned} \quad (45)$$

where m denotes the mth symbol period. The expression (45) is essentially the time reverse and conjugated version of the combination of the jth Walsh symbol code and the user spreading waveform for the mth symbol period. Note that the input data needs to be segmented into overlapping blocks of duration equal to one Walsh symbol plus the maximum multipath time delay spread commensurate with the operating environment. The overlap between adjacent blocks is equal to the maximum multipath time delay spread. Assume that for a given Walsh symbol period, we know, through either an initial setup or through past decisions, the indexes of the three previous Walsh symbols that were transmitted. These indexes are used to select the "correct" data for forming the spatial correlation matrix pencil $\{\hat{\mathbf{R}}_{S+I+N}, \hat{\mathbf{R}}_{I+N}\}$. A matrix beamformer composed of the $K_R < M$ "largest" eigenvectors of $\{\hat{\mathbf{R}}_{S+I+N}, \hat{\mathbf{R}}_{I+N}\}$, $\mathbf{w}_1, \mathbf{w}_2, \ldots, \mathbf{w}_{K_R}$ is applied to the "correct" data from the three previous Walsh symbol periods to transform to a K_R-dimensional beamspace where the MUAI should be dramatically reduced as a result of blindly placed spatial nulls [9], [10]. The beamspace-frequency correlation matrix pencil $\{\hat{\mathbf{K}}_{S+I+N}^r, \hat{\mathbf{K}}_{I+N}^r\}$ is then formed from the "correct" beamspace data in accordance with previous discussion. The "largest" generalized eigenvector of $\{\hat{\mathbf{K}}_{S+I}^r, \hat{\mathbf{K}}_I^r\}$ is applied to the frequency samples computed in the vicinity where the fingers are expected to occur, which is determined through approximate synchronization [6] and knowledge of the multipath time delay spread, for *each* of the Walsh function outputs associated with the "current" Walsh symbol period. The weighted sum having the largest magnitude dictates the estimate of the "current" Walsh symbol for forming subsequent estimates of $\{\hat{\mathbf{R}}_{S+I+N}, \hat{\mathbf{R}}_{I+N}\}$ and $\{\hat{\mathbf{K}}_{S+I+N}^r, \hat{\mathbf{K}}_{I+N}^r\}$ in a decision-directed fashion. The decision variable values $\|z_1\|^2, \|z_2\|^2, \ldots, \|z_{64}\|^2$ are fed to 64-ary decoder, deinterleaver, and Viterbi convolutional decoder.

VI. Simulations

A. Classical DS-CDMA

Example 1—Basic Performance of Blind 2-D RAKE Receiver: A linear array of eight antennas equispaced by a half wavelength was employed. Both the desired source and the interferers were DS-CDMA signals with different maximal length sequences and 127 chips per bit. A rectangular chip waveform was employed. The chip rate was 1 MHz, and the

[2]A blind initialization scheme is proposed in [15, ch. 5].

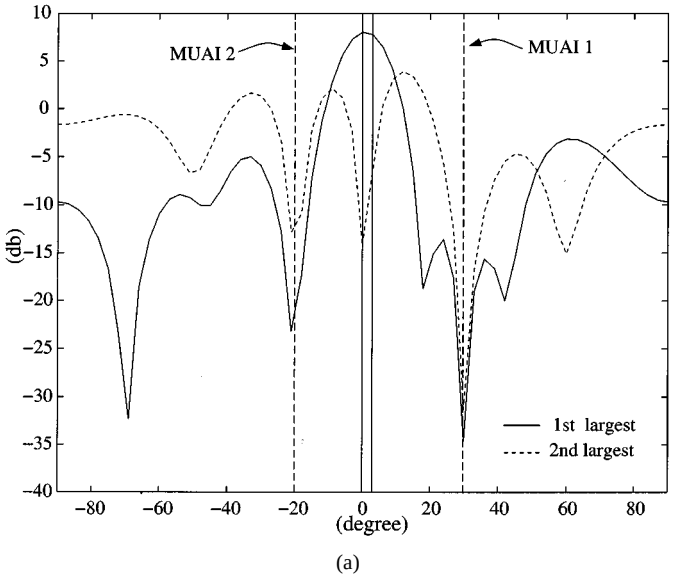

(a)

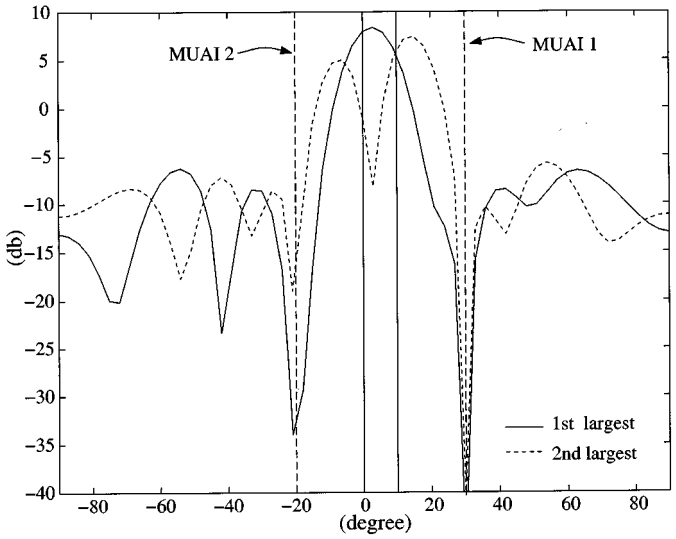

(b)

Fig. 4. Array patterns obtained with the spatial processing scheme. (a) A 3° separation case (BPSK). (b) A 10° separation case (BPSK).

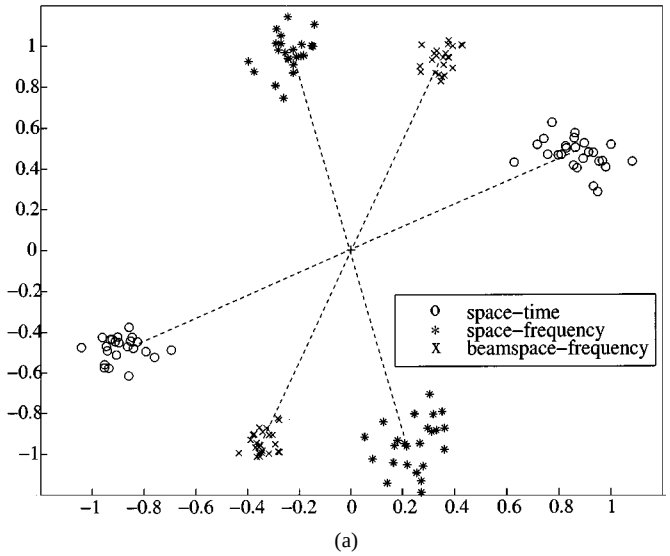

(a)

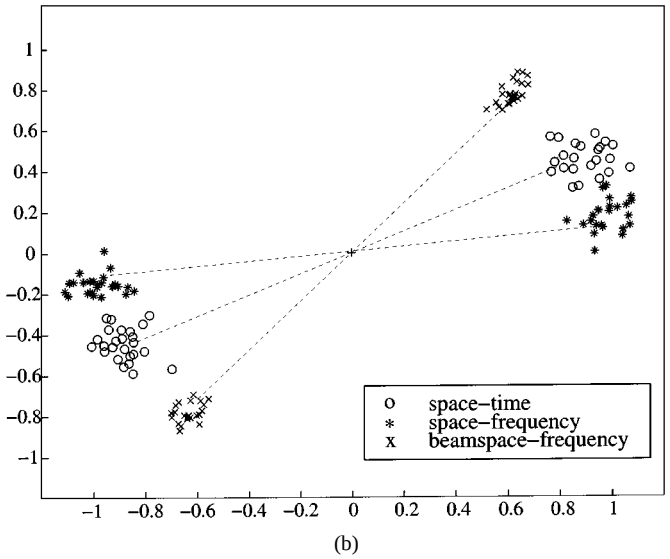

(b)

Fig. 5. Signal constellations of the three processing schemes and at one antenna (4 bits are averaged). (a) 3° separation case (BPSK). (b) 10° separation case (BPSK).

sampling rate was 2 MHz. A two-ray multipath model was used for the desired source wherein the direct path arrived at an angle of 0° relative to broadside with an SNR of -5 dB per element. The specular path was delayed by a half-chip and arrived at 10° or 3° with an SNR 6 dB below that of the direct path and phase shifted by 45° at the array center. The two DS-CDMA interferers arrived at 30° and $-20°$, respectively, with power levels of 20 dB and 25 dB above the desired user's direct path, respectively. The multipath delay spread was assumed to be 10 μs, dictating 20 half-chip spaced taps at each of the eight antennas. Thus, $\hat{\mathbf{K}}_{S+I+N}$ and $\hat{\mathbf{K}}_{I+N}$ were 160×160. Note that for estimating $\hat{\mathbf{K}}_{I+N}$, we extracted 72 snapshots per bit interval over that portion away from "RAKE fingers" by sliding the 10-μs time window over a chip per time. The beam pattern obtained with the weight vector $\mathbf{w}$ computed as the "largest" generalized eigenvector of the matrix pencil $\{\hat{\mathbf{R}}_{S+I+N}, \hat{\mathbf{R}}_{I+N}\}$ is plotted as the solid curve in Fig. 4(a) and (b) for the respective cases of 3° and 10° multipath angular spreads. In each case, the pattern is observed to peak at the angular direction of the direct path, have substantial gain in the direction of the specular path, and have a deep null in the direction of each MUAI.

The case of 10° angular separation between the two multipaths is a borderline space-resolvable scenario. In this case, the beampattern obtained with the second "largest" generalized eigenvector of the matrix pencil $\{\hat{\mathbf{R}}_{S+I+N}, \hat{\mathbf{R}}_{I+N}\}$ is plotted as the dash curve in Fig. 4(b). It is observed to yield a null in the direct path direction, as well as a null in the direction of the interferer. Thus, for the reduced-dimension processor, two beams encompassing the angular spread of the desired user's multipath were formed (blindly) from the two "largest" generalized eigenvectors of the 8×8 spatial correlation matrix pencil $\{\hat{\mathbf{R}}_{S+I+N}, \hat{\mathbf{R}}_{I+N}\}$. In addition, for each bit period at each antenna, a 20-point DFT of the 20 samples encompassing the multipath spread were computed, but only the $K_C = 9$ frequency samples centered at DC were retained for the reduced dimension space-time RAKE receiver. Thus, $\mathbf{T}^{rH}\hat{\mathbf{K}}_{S+I+N}\mathbf{T}^{r}$ and $\mathbf{T}^{rH}\hat{\mathbf{K}}_{I+N}\mathbf{T}^{r}$ were 18×18. Applying

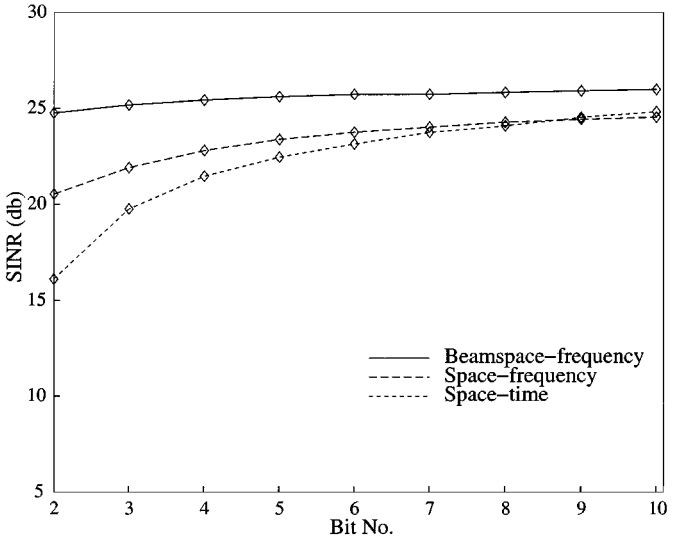

Fig. 6. Performance comparison with varying bit number for processing (BPSC).

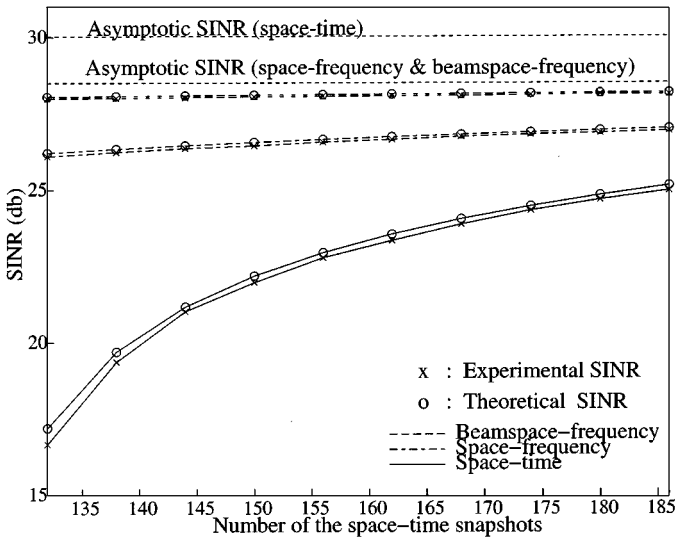

Fig. 7. Simulation result for the verification of the design of the compression matrix.

the space-time, space-frequency, and beamspace-frequency processing schemes yielded the signal constellations plotted in Fig. 5(a). Four bits were averaged to estimate the "optimal" weight vector for each processing scheme. This set of weights was then applied to each of 44 successive bit periods; the results are overlaid. The computational reduction was from a 160×160 space-time matrix pencil, to a 72×72 space-frequency matrix pencil, to an 18×18 beamspace-frequency matrix pencil.

In contrast, as the 3–dB beamwidth for the eight-element array is roughly 15°, the multipaths separated by 3° are not resolvable in space for all practical purposes. Only the "largest" generalized eigenvector is employed yielding a beamspace of dimension one. In this case, we need only effect a 1-D blind RAKE receiver in the frequency domain wherein the matrices are of dimension 9×9. Doing so yielded the signal constellation plotted in Fig. 5(b). Of course, in both Fig. 5(a) and (b), there is an rotation of the constellation due to the blind nature of the algorithm.

Example 2—Performance for Classical DS-CDMA Comparing Full Dimension Space-Time Processing, Temporal-Only Compression, and Spatio-Temporal Compression: To illustrate the performance in terms of output SINR among these three processing schemes, we created a different simulation scenario from the first example for fair comparison. A three-ray multipath model was used for the desired source wherein the direct path arrived at an angle of 0° relative to broadside with an SNR of -5 dB per element. The SNR of the specular multipaths were 3 and 6 dB below that of the direct path and phase shifted by 45° and 90° at the first antenna element. The specular path for the SOI arrived at 3° delayed by four and a half chips, and the other arrived at 10° delayed by seven chips. The two DS-CDMA interferers arrived with the same setup as before. The multipath delay spread was assumed to be 8 μs, dictating 16 half-chip spaced taps at each of the eight antennas. Thus, $\hat{\mathbf{K}}_{S+I+N}$ and $\hat{\mathbf{K}}_{I+N}$ were 128×128. Although the space-frequency correlation matrices were 56×56, the beamspace-frequency correlation matrices were 14×14 since seven frequency samples centered at DC were retained from the 16-point DFT, and two beams were formed from the two "largest" generalized eigenvectors of the 8×8 spatial correlation matrix pencil $\{\hat{\mathbf{R}}_{S+I+N}, \hat{\mathbf{R}}_{I+N}\}$. Fig. 6 shows the sample mean, obtained by averaging over 256 independent trial runs, of the output SINR as a function of the number of bits over which $\hat{\mathbf{K}}_{S+I+N}$ and $\hat{\mathbf{K}}_{I+N}$ were averaged. The reduced dimension space-time RAKE receiver is observed to yield a much larger output SINR when averaging over only a small number of bit periods.

Example 3—Verification of the Design of the Compression Matrix: The simulation scenario was the same as in Example 2. This simulation example serves to demonstrate that the data dependent dimensionality reducing matrix $\mathbf{T}^r$ is well designed, as discussed in Section III-B. For this purpose, we assumed the post-correlation space-time signature of the desired user $\mathbf{d}$ was known and compared the output SINR obtained with $\hat{\mathbf{w}} = \hat{\mathbf{K}}_I^{-1}\mathbf{d}$ with that obtained with $\hat{\mathbf{w}}^r = \{\mathbf{T}^{rH}\hat{\mathbf{K}}_I\mathbf{T}^r\}^{-1}\{\mathbf{T}^{rH}\mathbf{d}\}$ for a finite sample size. In order to make the assumptions valid for using (41), we extracted only six independent snapshots per bit interval by sliding the time window 16 samples per time and generated a number of bits varying from 22 to 31 (132 to 186 snapshots—such that the number of snapshots is greater than the dimension of space-time correlation matrix, which equals 128 in this example) in estimating $\hat{\mathbf{K}}_{I+N}$. We also assumed each snapshot contributed from the interference plus noise after the matched filter has having approximately a Gaussian distribution $\sim \mathcal{N}(\mathbf{0}, \mathbf{K}_{I+N})$. Fig. 7 shows the sample mean obtained by averaging over 256 independent trial runs of the output SINR as a function of the number of the snapshots over which $\hat{\mathbf{K}}_{I+N}$ was averaged. The theoretical output SINR curves were generated using the formula in (41). The results show that the values of the experimental output SINR and theoretical output SINR are approximately equal, and our compression matrix $\mathbf{T}^r$ is judiciously designed, yielding a larger output SINR for a finite sample size. The average loss in the asymptotic SINR of the reduced dimension processing is approximately 1.5 dB. The difference in the asymptotic SINR between the space-frequency and the beamspace-frequency schemes is very small (less than

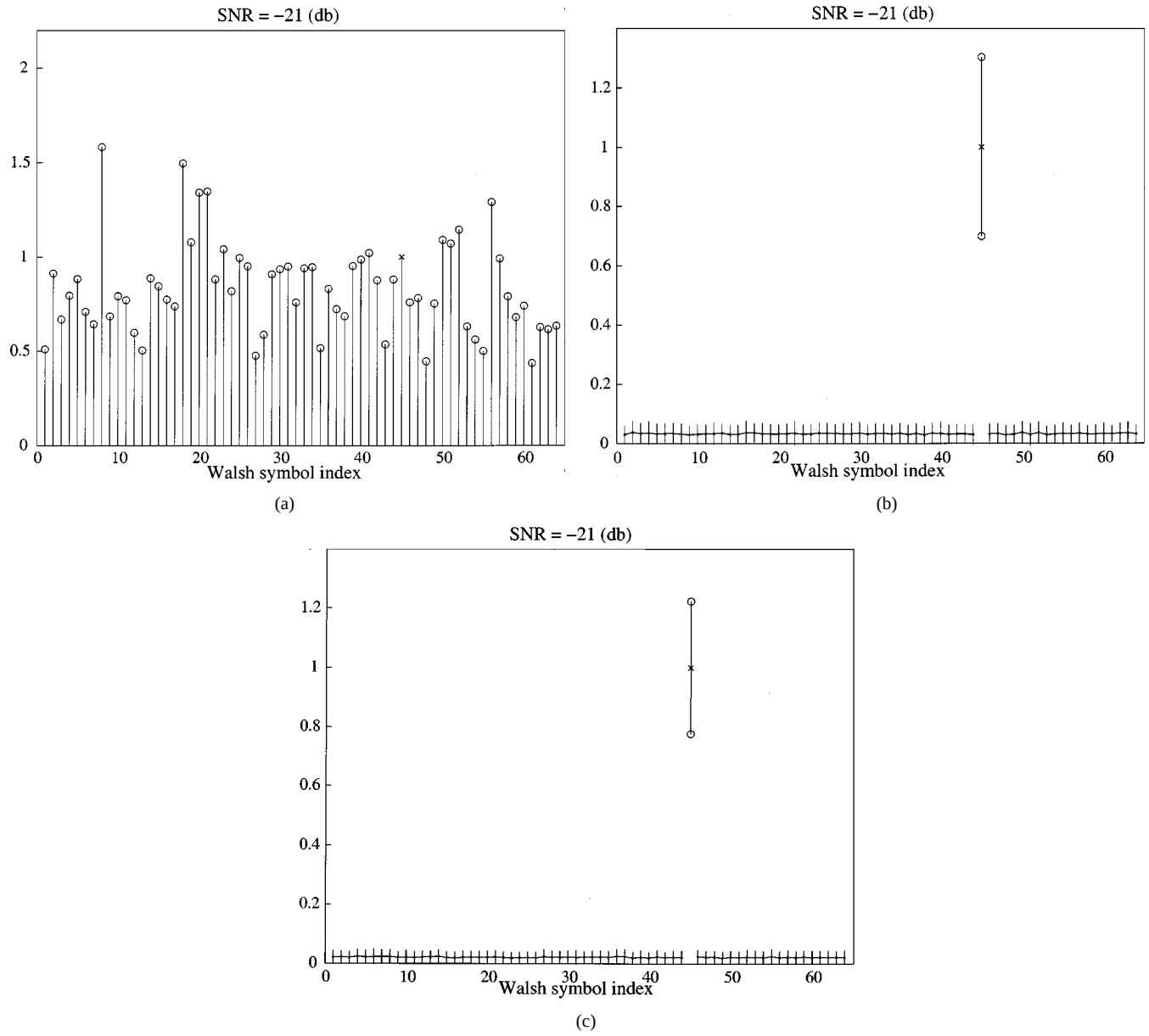

Fig. 8. Decision variables for the IS-95 uplink—Mean and standard. (a) One antenna (single run). (b) Space-time processing. (c) Beamspace-frequency processing.

0.05 db) and is indistinguishable in the plot. Note that the loss incurred in this simulation example was determined to be 0.8 dB when using only nine frequency samples.

B. IS-95 Uplink

In the simulation examples for IS-95 uplink, we employed the following parameters. The time between chips is 0.8138 μs; the sampling rate was twice the chip rate. The number of half-chip spaced taps at each antenna used to encompass the delay spread was 16. The number of selected DFT samples was nine, and $M = 9$ antennas were used. The dimension of the beamspace was equal to 2. A three-ray multipath model was used for the desired user, wherein the direct path arrived at an angle of 0° relative to broadside. The SNR's of the two specular multipaths were 1 dB and 3 dB below that the direct path and phase shifted by 45° and 90° at the array center, respectively. The relative delays of the specular multipaths for the desired source were 1.5 chips and four chips respectively; the angles were 3° and 10°, respectively. The parameters for the MUAI's are listed in Table II. To simulate multipath, each MUAI arrived via two paths having distinct arrival angles, time delays, and phase shifts. Both the desired source and the interferers were DS-CDMA signals with different long PN codes and the same short I-Q PN codes. These different long PN codes were effectively generated from the same generating polynomial with different initial states. The generating polynomials for the long and short PN sequences are listed below [11].

$$\begin{aligned} g_L(x) &= x^{42} + x^{35} + x^{33} + x^{31} + x^{27} + x^{26} + x^{25} \\ &\quad + x^{22} + x^{21} + x^{19} + x^{18} + x^{17} + x^{16} + x^{10} \\ &\quad + x^7 + x^6 + x^5 + x^3 + x^2 + x^1 + 1 \\ g_I(x) &= x^{15} + x^{13} + x^9 + x^8 + x^7 + x^5 + 1 \\ g_Q(x) &= x^{15} + x^{12} + x^{11} + x^{10} + x^6 + x^5 + x^4 + x^3 + 1. \end{aligned}$$

Note that for estimating $\mathbf{K}_I$, we extracted 200 snapshots per bit interval by sliding the time window over one chip per time in the

TABLE I
LIST OF INTEGER-VALUED PARAMETERS

M:	number of antennas
P:	number of dominant mutipaths for the Signal of Interest (SOI)
J:	number of dominant co-channel MUAI's
N_b:	number of bits for which multipath scenario stays constant
N_c:	number of chips per bit common to all sources
L_c:	number of samples per chip
N_s:	$= L_c\tau_{max}/T_c$ = number of samples encompassing multipath delay spread
N:	$= MN_s$ = dimension of space-time snapshots and correlation matrices
K_C:	number of spectral lines used in reduced dimension processing (see Sect. 3.1.3)
K_R:	number of beams used in reduced dimension processing (see Sect. 3.2.2)

TABLE II
SIGNAL AND MUAI PARAMETERS

	Signal	MUAI1	MUAI2	MUAI3
SNR 1,2,3 (db)	x,x-1,x-3	x+20,x+10, -	x+4,x+6, -	x,x-3, -
Phase 1,2,3	$0^o, 45^o, 90^o$	$45^o, 50^o, -$	$-30^o, -35^o, -$	$180^o, 170^o, -$
DOA 1,2,3	$0^o, 3^o, 10^o$	$30^o, 35^o, -$	$-20^o, -23^o, -$	$-10^o, -7^o, -$
Delay 1,2,3 ($\times\frac{1}{2}T_c$)	0,3,8	0, 3, –	0, 6, –	0, 10, –

following simulations, and the number of these snapshots can be adjusted equal to, for example, 50, for reducing computations and real-time implementation.

Example 1—Performance of the Proposed 2-D RAKE Receiver for the IS-95 Uplink: If there were no multipath, no MUAI's, and no noise, the 64 decision variables for a given symbol period would ideally be a scalar multiple of the 64×1 vector $(0, 0, \ldots, 1, \ldots, 0)$, where the 1 is located in the position index of the actual Walsh symbol sent during that period. Fig. 8(a) plots the values of the 64 decision variables for a Walsh symbol period obtained by using the incoherent square-law combining RAKE receiver at one of the antennas using only those three time samples corresponding to the exact multipath arrival times. The value of each decision variable was divided by the value of the decision variable associated with the correct Walsh symbol whose index is marked "x" in Fig. 8(a). A dramatic improvement is observed relative to Fig. 8(a) as a result of the MUAI cancellation effected by the 2-D space-time space processing either in full dimension or reduced dimension. Fig. 8(b) and (c) display the means (connected by the horizontal line) and standard deviations (vertical lines) of the respective magnitude of each of the 64 Walsh symbol decision variables for the "one-shot" decision-directed 2-D RAKE receiver proposed in this paper averaged over 256 independent runs conducted at input SNR $x = -21$ db. Once the first three Walsh symbols were estimated through our initialization algorithm, $\hat{\mathbf{K}}_{S+I+N}$ and $\hat{\mathbf{K}}_{I+N}$ were averaged over the three past Walsh symbol periods, and the "largest" generalized eigenvector was applied to each output of the 64 matched filters in the "fingers" region for estimating the fourth Walsh symbol. Note that we fixed the fourth Walsh symbol with index 45 to be transmitted in order for the sake of illustration. Reduced-dimension processing is observed to yield a substantially better separation between the value of the true Walsh symbol decision variable and the other 63 decision variables.

Example 2—Time-Varying Channel Simulation Involving Moving Mobile: In all of the simulations presented thus far, we essentially assumed the channel was invariant over a four Walsh symbol duration. For the case of a time-varying channel, the "three-Walsh-symbol" time window is shifted over one Walsh symbol at a time to update the matrix pencil for computing the space-time RAKE receiver taps for estimating the "new" Walsh symbol. To create a time-varying scenario, the signal and interference parameters were set equal to those listed in Table I with an input SNR of $x = -21$ dB; the mobile was then set in motion at 75 MPH toward the base. This induced a different Doppler shift on each multipath. The fact that the channel varied substantially over a block of 200 Walsh symbols may be observed in Fig. 9(a). The magnitude of the frequency response of the channel associated with the first antenna occurring during the fifth Walsh symbol period is plotted, along with that occurring during the 190th Walsh symbol period. Despite the substantial change in the channel from the beginning of the 200 symbol burst to the end, the output SINR of the reduced dimension 2-D RAKE receiver plotted in Fig. 9(b) is observed to be relatively constant over the 200 symbol burst and nearly equal to the asymptotic beamspace-frequency SINR. Thus,

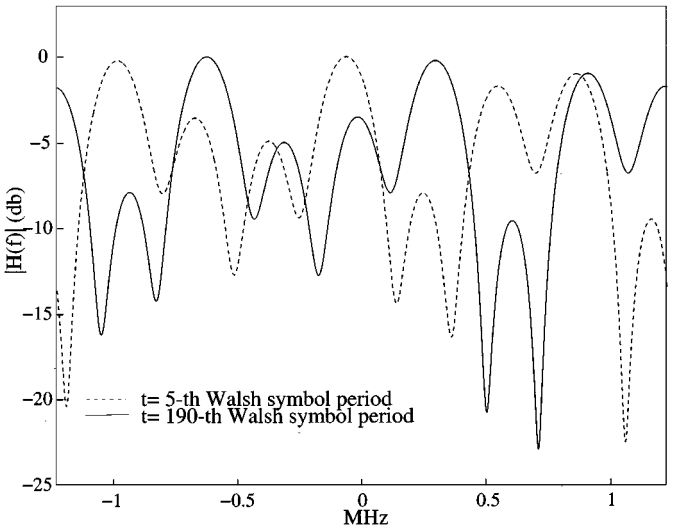

(a)

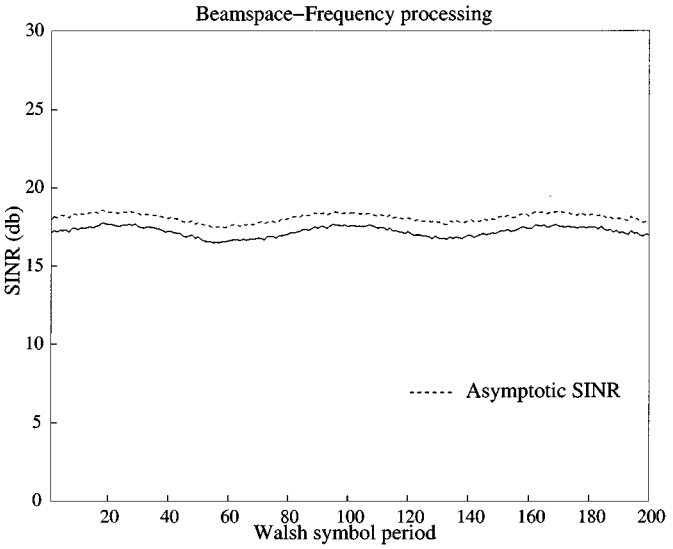

(b)

Fig. 9. Time-varying channel example. (a) Channel frequency response at different symbol periods. (b) Mean of SINR of 40 independent runs.

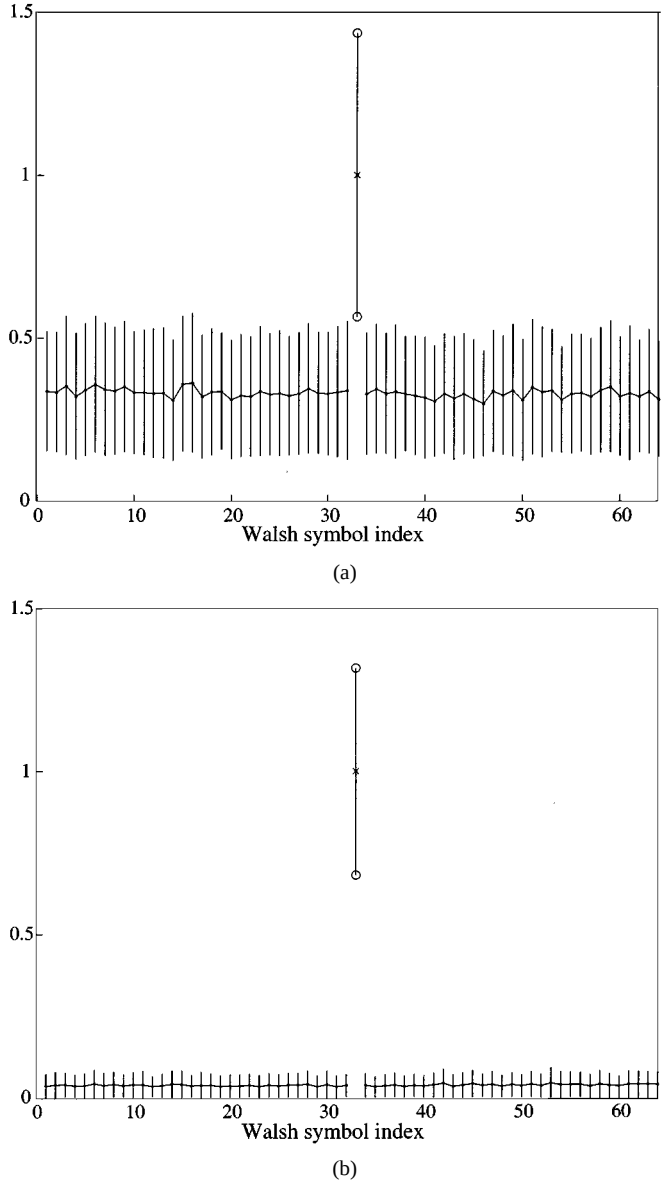

Fig. 10. Decision variables for the IS-95 uplink with equal power scenario—mean and std.

for the IS-95 uplink, the "three-Walsh-symbol" time window appears to work quite well for achieving near maximum output SINR under rapidly time-varying channel conditions.

Example 3—Performance Comparison with Power Control—Reduced-Dimension 2–D RAKE Receiver versus Conventional 1-D RAKE Receiver: Here, we create a simulation scenario with equal input power for all the co-channel users for performance comparison. $M = 8$ antennas were used. The signal of the desired user is the same as that in Example 1. The input SNR x of the direct path was equal to -21 db. Forty users with different PN codes and single path were created with input SNR equal to -21 db, and the AOA's were uniformly distributed within 120°. We conducted 256 independent runs. The results in Fig. 10(a) and (b) reveal that the reduced-dimension 2-D RAKE receiver achieved much better performance than the 1-D incoherent combining RAKE receiver. The incoherent combining 1-D RAKE receiver made 212 detection errors out of 256 trial runs when the input SNR of only one user was 20 db above the direct path of the desired user.

VII. Summary and Conclusions

Blind reduced-dimension 2-D RAKE receivers that only require knowledge of the spreading waveform of the desired user and approximate bit synchronization were developed based on a novel frequency domain implementation of a RAKE receiver and beamspace transformations. The advantages of the reduction in dimensionality include reduced computational complexity and faster convergence at the cost of only a slight drop in asymptotic SNR relative to the full-dimension space-time RAKE receiver. A decision-directed adaptation was developed for the IS-95 uplink. Simulations reveal the proposed scheme to provide near coherent combining of the desired user's multipath while simultaneously canceling strong MUAI's and good tracking ability.

References

[1] U. Madhow and M. Honig, "MMSE interference suppression for direct-sequence spread spectrum CDMA," *IEEE Trans. Commun.*, vol. 42, pp. 3178–3188, 1994.

[2] A. Naguib, A. Paulraj, and T. Kailath, "Capacity improvement with base-station antenna array in cellular CDMA," *IEEE Trans. Veh. Technol.*, vol. 43, pp. 691–698, Aug. 1994.

[3] A. Naguib and A. Paulraj, "Performance of CDMA cellular networks with base-station antenna arrays," in *Proc. Int. Zurich Seminar Digital Commun.*, Mar. 1994, pp. 87–100.

[4] H. Liu and M. D. Zoltowski, "Blind equalization in antenna array CDMA systems," *IEEE Trans. Signal Processing*, pp. 161–172, Jan. 1997.

[5] T. F. Wong, T. M. Lok, J. S. Lehnert, and M. D. Zoltowski, "A unified linear receiver for direct-sequence spread-spectrum multiple access systems with antenna arrays and blind adaptation," *IEEE Trans. Inform. Theory*, vol. 44, pp. 659–676, Mar. 1998.

[6] J. Ramos, M. D. Zoltowski, and H. Liu, "A low complexity space-time processor for DS-CDMA communications," *IEEE Signal Processing Lett.*, pp. 262–265, Sept. 1997.

[7] B. Suard, A. Naguib, G. Xu, and T. Kailath, "Performance analysis of CDMA mobile communication systems using antenna arrays," in *Proc. Int. Conf. Acoust. Speech, Signal Process.*, vol. VI, Apr. 1993, pp. 153–156.

[8] T. S. Rappaport, S. Y. Seidel, and S. Yoshida, "900 MHz multipath propagation measurements for U.S. digital cellular radiotelephone," *Proc. IEEE Globecom*, pp. 84–89, 1989.

[9] M. D. Zoltowski and J. Ramos, "Blind multi-user access interference cancellation for CDMA based PCS/cellular using antenna arrays," in *Proc. IEEE ICASSP*, May 1996, pp. 2730–2733.

[10] "Blind adaptive beam forming for CDMA based PCS/cellular," in *Proc. Conf. Rec. 29th Asilomar IEEE Conf. Signals, Syst., Comput.*, Nov. 1995, pp. 378–382.

[11] M. D. Zoltowski, Y.-F. Chen, and J. Ramos, "Blind 2D RAKE receivers based on space-time adaptive MVDR processing for the IS-95 cdma system," in *Proc. Milcom*, Oct. 1996, pp. 618–622.

[12] Y.-F. Chen and M. D. Zoltowski, "Convergence analysis and tracking ability of reduced dimension blind space-time rake receivers for DS-CDMA," in *Proc. Veh. Technol. Conf.*, May 1998, pp. 2333–2337.

[13] A. F. Naguib and A. Paulraj, "A base-station antenna array receiver for cellular DS/CDMA with M-ary orthogonal modulation," in *Proc. IEEE 28th Asilomar Conf.*, Nov. 1994, pp. 858–862.

[14] S. Haykin and A. Steinhardt, *Adaptive Radar Detection Estimation*. New York: Wiley, 1992, p. 132.

[15] Y.-F. Chen, "Space-time adaptive processing for DS-CDMA communication systems," Ph.D. dissertation, Purdue Univ., West Lafayette, IN, Aug. 1998.

Yung-Fang Chen was born in Taipei, Taiwan, R.O.C., in 1968. He received the B.S. degree in computer science and information engineering from National Taiwan University, Taipei, in 1990, the M.S. degree in electrical engineering from the University of Maryland, College Park, in 1994 and the Ph.D. degree in electrical engineering from Purdue University, West Lafayette, IN, in 1998.

From 1990 to 1992, he served in the Taiwan Army as a Second Lieutenant. Since September 1998, he has been a Communications Engineer for Lucent Technologies, Whippany, NJ. His areas of interest include space-time adaptive processing for DS-CDMA communication systems and space-time processing for third-generation wireless networks.

Michael D. Zoltowski (F'99) was born in Philadelphia, PA, on August 12, 1960. He received both the B.S. and M.S. degrees in electrical engineering with highest honors from Drexel University, Philadelphia, in 1983 and the Ph.D. degree, in systems engineering from the University of Pennsylvania, Philadelphia, in 1986.

From 1982 to 1986, he was an Office of Naval Research Graduate Fellow. In Fall 1986, he joined the faculty of Purdue University, West Lafayette, IN, where he currently is Professor of electrical and computer engineering. During 1987, he held a position of Summer Faculty Research Fellow at the Naval Ocean Systems Center, San Diego, CA. He is a contributing author to *Adaptive Radar Detection and Estimation* (New York: Wiley, 1991), *Advances in Spectrum Analysis and Array Processing, Vol. III* (Englewood Cliffs, NJ: Prentice-Hall, 1994), and *CRC Handbook on Digital Signal Processing* (Boca Raton, FL: CRC, 1996). His present research interests include space-time adaptive processing and blind antenna array beamforming for all areas of mobile and wireless communications, radar, and GPS.

Dr. Zoltowski was the recipient of the IEEE Outstanding Branch Counselor Award for 1989–1990, the Ruth and Joel Spira Outstanding Teacher Award for 1990–1991, and the IEEE Signal Processing Society's 1991 Paper Award (Statistical Signal and Array Processing Technical Area). He is the recipient of "The Fred Ellersick MILCOM Award for Best Paper in the Unclassified Technical Program" at the IEEE Military Communications (MILCOM'98) Conference. He has served as an Associate Editor for the IEEE TRANSACTIONS ON SIGNAL PROCESSING and an Associate Editor for the IEEE COMMUNICATIONS LETTERS. Within the IEEE Signal Processing Society, he has been a Member of the Technical Committee for the Statistical Signal and Array Processing Area and is currently a member of the Technical Committee for Communications and the Technical Committee on Education. In addition, he is currently a Member-at-Large of the Board of Governors and Secretary of the IEEE Signal Processing Society.

Javier Ramos received the B.Sc., M.Sc. and the Ph.D. degrees from the Polytechnic University of Madrid, Madrid, Spain, in 1987, 1989, and 1995, respectively. During his Ph.D. studies, he actively cooperated in several research projects at Purdue University, West Lafayette, IN.

In 1996, he was Post-Doctoral Research Associate at Purdue University. During 1997, he was Assistant Professor at the Polytechnic University of Madrid. In 1998, he joined Carlos III University, Madrid, where he is an Associate Professor. His areas of research include third generation of mobile communications, array processing, digital communications, spread spectrum systems, and applications such as GPS and cellular systems.

Dr. Ramos received the Ericsson award for the best Ph.D. dissertation on digital communications in 1996.

Chanchal Chatterjee received the B.Tech. degree in electrical engineering from the Indian Institute of Technology, Kanpur, in 1983 and the M.S.E.E. and Ph.D. degrees in electrical and computer engineering from Purdue University, West Lafayette, IN, in 1984 and 1996, respectively.

Between 1985 and 1995, he worked at Machine Vision International and Medar, Inc., Detroit, MI. He is currently Senior Algorithms Specialist with GDE Systems, Inc., San Diego, CA. He is also affiliated with the Department of Electrical Engineering, University of California, Los Angeles. His areas of interest include image processing, computer vision, neural networks, and adaptive algorithms and systems for pattern recognition and signal processing.

Vwani P. Roychowdhury received the Ph.D. in electrical engineering from Stanford University, Stanford, CA, in 1989.

From 1991 to 1996, he was a faculty member with the School of Electrical and Computer Engineering, Purdue University, West Lafayette, IN, where he was promoted to Associate Professor in 1995. In 1996, he joined the University of California, Los Angeles, where he is currently a Professor of electrical engineering. His research interests include models of computation, quantum and nanoelectronic computation, quantum information processing, fault-tolerant computation, combinatorics and information theory, advanced statistical processing, and adaptive algorithms. He has co-authored several books including *Discrete Neural Computation: A Theoretical Foundation* (Englewood Cliffs, NJ: Prentice-Hall, 1995) and *Theoretical Advances in Neural Computation and Learning* (Boston, MA: Kluwer, 1994).

Dr. Roychowdhury was a General Motors Faculty Fellow at Purdue University from 1992 until 1994 and was awarded the Ruth and Joel Spira Outstanding Teacher Award in 1994. He received the 1999 Best Paper Award from the IEEE TRANSACTIONS ON NEURAL NETWORKS.